# ARTICLE IN PRESS

Bioactive Materials xxx (xxxx) xxx

KeA1

CHINESE ROOTS
GLOBAL IMPACT

Contents lists available at ScienceDirect

# **Bioactive Materials**

journal homepage: www.keaipublishing.com/en/journals/bioactive-materials



# Supramolecular hybrid hydrogels as rapidly on-demand dissoluble, self-healing, and biocompatible burn dressings

A. Aslihan Gokaltun <sup>a,b,c,d</sup>, Letao Fan <sup>a,b</sup>, Luca Mazzaferro <sup>c</sup>, Delaney Byrne <sup>a,b</sup>, Martin L. Yarmush <sup>a,b,e</sup>, Tianhong Dai <sup>f</sup>, Ayse Asatekin <sup>c,\*\*</sup>, O. Berk Usta <sup>a,b,\*</sup>

- a Center for Engineering in Medicine and Surgery, Massachusetts General Hospital, Harvard Medical School, 55 Fruit St., Boston, MA, 02114, USA
- <sup>b</sup> Shriners Hospitals for Children, 51 Blossom St., Boston, MA, 02114, USA
- <sup>c</sup> Department of Chemical and Biological Engineering, Tufts University, 4 Colby St., Medford, MA, 02474, USA
- <sup>d</sup> Department of Chemical Engineering, Hacettepe University, 06532, Beytepe, Ankara, Turkey
- e Department of Biomedical Engineering, Rutgers University, 599 Taylor Rd., Piscataway, NJ, 08854, USA
- f Wellman Center for Photomedicine, Massachusetts General Hospital, Department of Dermatology, Harvard Medical School, 50 Blossom Street, Boston, MA, 02114, USA

#### ARTICLE INFO

# Keywords: Supramolecular hybrid hydrogels Cationic copolymer On-demand dissoluble Self-healable Biocompatible Burn injury

#### ABSTRACT

Despite decades of efforts, state-of-the-art synthetic burn dressings to treat partial-thickness burns are still far from ideal. Current dressings adhere to the wound and necessitate debridement. This work describes the first "supramolecular hybrid hydrogel (SHH)" burn dressing that is biocompatible, self-healable, and on-demand dissoluble for easy and trauma-free removal, prepared by a simple, fast, and scalable method. These SHHs leverage the interactions of a custom-designed cationic copolymer via host-guest chemistry with cucurbit[7]uril and electrostatic interactions with clay nanosheets coated with an anionic polymer to achieve enhanced mechanical properties and fast on-demand dissolution. The SHHs show high mechanical strength (>50 kPa), self-heal rapidly in ~1 min, and dissolve quickly (4–6 min) using an amantadine hydrochloride (AH) solution that breaks the supramolecular interactions in the SHHs. Neither the SHHs nor the AH solution has any adverse effects on human dermal fibroblasts or epidermal keratinocytes *in vitro*. The SHHs also do not elicit any significant cytokine response *in vitro*. Furthermore, *in vivo* murine experiments show no immune or inflammatory cell infiltration in the subcutaneous tissue and no change in circulatory cytokines compared to sham controls. Thus, these SHHs present excellent burn dressing candidates to reduce the time of pain and time associated with dressing changes.

# 1. Introduction

Burn injuries are devastating and demanding critical care problems and present a major public health predicament, especially in low and middle-income countries [1,2]. Burn injuries are the fourth most common type of trauma globally and among the most complicated to manage [3]. Even in the United States,  $\sim 500,000$  burn injuries that are severe enough to require treatment occur each year [4]. The direct medical costs for caring for these patients in the US were  $\sim $1.5$  billion, and the associated indirect costs with burns exceeded \$5 billion in 2013 [5]. Various wound dressings exist in the clinic to treat partial-thickness

burns [6]. Yet, they are far from ideal, and none of them are considered the "gold standard." Among these, hydrogel dressings have emerged as a critical alternative to promoting healthy and timely wound healing since they can absorb the wound exudate, provide a moist environment for the wound, and prevent bacterial infections via embedded moieties. However, they adhere to the wound and need to be mechanically or surgically debrided, leading to the traumatization of newly epithelialized tissues, delayed healing, and severe pain for the patient [7].

Burn dressing removal is reported to be the time of most pain (after the burn), and opioids have, thus, become the cornerstone of burn wound treatment [8]. The average burn dressing change in a typical

Peer review under responsibility of KeAi Communications Co., Ltd.

E-mail addresses: Ayse.Asatekin@tufts.edu (A. Asatekin), ousta@mgh.harvard.edu (O.B. Usta).

#### https://doi.org/10.1016/j.bioactmat.2022.09.003

Received 25 May 2022; Received in revised form 15 August 2022; Accepted 5 September 2022 Available online 27 September 2022

2452-199X/© 2022 The Authors. Publishing services by Elsevier B.V. on behalf of KeAi Communications Co. Ltd. This is an open access article under the CC BY-NC-ND license (http://creativecommons.org/licenses/by-nc-nd/4.0/).

Please cite this article as: A. Aslihan Gokaltun, Bioactive Materials, https://doi.org/10.1016/j.bioactmat.2022.09.003

<sup>\*</sup> Corresponding author. Center for Engineering in Medicine and Surgery, Massachusetts General Hospital, Harvard Medical School, 55 Fruit St., Boston, MA, 02114, USA.

<sup>\*\*</sup> Corresponding author.

injury requiring ICU level care takes  $\sim$ 57 min with anesthesia and can extend to over 3 h. For example, it takes three people 138 min to dress for a 10–30% burn, 105 min for a facial burn, and 66 min for a hand dressing change [9]. Anesthesia further increases the time and complexity [9,10]. Hence, novel alternative hydrogels that enable easy and pain-free dressing changes while minimizing procedural tissue damage are urgently needed.

On-demand dissoluble hydrogels are a particularly interesting class of wound dressings, as the on-demand dissolution would i) ease the removal of the dressing, ii) require no additional mechanical and/or surgical debridement, iii) reduce dressing change time, and iv) minimize painful procedures. So far, on-demand dissoluble hydrogels have been reported based on chemically crosslinked hydrogels (CCHs) [11-18] or physically crosslinked hydrogels (PCHs) [19]. CCHs utilize cleavable moieties that can undergo degradation through chemical or enzymatic reactions [20]. This results in long-dissolution times (>30 min) [11, 13-15,21-23] and involves toxic compounds or side reactions when used in wound care. On the other hand, PCHs can be dissolved via various stimuli (e.g., pH or temperature) [24]. However, their clinical adoption is hindered by their poor mechanical properties [24]. Moreover, these traditional approaches comprise complicated processing steps during hydrogel synthesis rendering them unfavorable for large-scale production, and lack in vivo and in vitro data to gauge the biocompatibility and clinical relevance of such hydrogels in burn care [11,12,19,24]. Although promising progress has been made on on-demand dissoluble hydrogels for burn wound care [11,12,18,19], these numerous hurdles have made the on-demand dissolution of hydrogels elusive in practice (Table 1). Further research and development are assuredly needed to facilitate the clinical translation and adoption of such hydrogels.

Supramolecular hydrogels (SHs), a novel class of PCHs, are held together by non-covalent crosslinks such as host-guest chemistry, electrostatic interactions, and hydrogen bonding [25]. These interactions eliminate the need for several synthesis steps and challenging purification procedures [26]. Host-guest chemistry is a rapidly expanding approach for building SHs where two or more molecules with unique structural connections and noncovalent binding can create complexes. Host-guest chemistry is highly versatile due to its specificity, interaction strength, and controlled reversibility [27]. Crown ethers, cucurbit[n] urils (CBs), calix[n]arenes, pillar[n]arenes, and cyclodextrins (CDs) are macrocyclic molecules used as hosts to encapsulate smaller organic molecules (guests) in host-guest chemistry [26]. Among these, CBs and CDs have been widely preferred as hosts since they exhibit good

biocompatibilities in the biomedical field. CBs can form stable complexes with guests in an aqueous solution with high binding affinities (as high as  $10^{17}\,\mathrm{M}^{-1}$ , equivalent to that of the avidin–biotin host–guest pair [28]), which is a distinct advantage compared to CDs. The low binding constants of CDs (10 [3]– $10^5\,\mathrm{M}^{-1}$ ) necessitate excessive concentrations of CDs to quantitatively form host-guest complexes [29].

Unlike most synthetic hydrogels with permanent chemical crosslinks, SHs can undergo dissolution in response to various environmental stimuli and self-heal when damaged [30–32]. SHs that rely on host-guest chemistry can easily be dissembled by adding a compound that has a very high affinity to a host and can break the physical crosslinks, serving as a dissolution agent (DSA). However, while SHs display unique dynamic features, their mechanical properties are often inadequate for clinical use. Integration of benign inorganic materials (*i.e.*, clay) to form supramolecular "hybrid" hydrogels (SHHs) can improve mechanical properties beyond SHs [33–37]. This approach has not yet been explored in the context of dissolvable burn dressings.

Here, we designed and synthesized the first supramolecular "hybrid" hydrogel (SHH) for treating second-degree burns. Our design goals for this SHH were a) simple fabrication, b) rapid on-demand dissolution for easy removal, c) high mechanical toughness, d) rapid, autonomous selfhealing, and e) high biocompatibility in vitro and in vivo. Our synthesis approach does not require any toxic compounds, catalysts, and initiators, unlike the commonly used CCHs, and thus advances "green chemistry" strategies [38-41]. Specifically, our SHH comprises four main components: 1) a water-soluble cationic copolymer (CP) (guest), 2) cucurbit[7]uril (CB[7]) molecules (host), 3) exfoliated clay nanosheets (CNSs), and 4) sodium polyacrylate (SPA, anionic) (Fig. 1A). We first designed and synthesized water-soluble acrylamide-random-[3-(methacryloylamino)propyl]trimethylammonium chloride (Am-r-MATMAC) copolymers (CPs) such that this cationic CP guest can strongly interact with the highly electronegative portals of CB[7] host molecules. Then, we combined CB[7] and the CP with inorganic clay nanosheets (CNSs) stabilized with sodium polyacrylate (SPA) to improve SHH mechanical properties (Fig. 1B).

The combination of these four components, *i.e.*, the host, the guest, and the SPA-stabilized exfoliated CNSs, resulted in mechanically strong and stable supramolecular hybrid hydrogels in less than a minute. Importantly, these SHHs are also easily and rapidly dissoluble by a dissolution agent, amantadine hydrochloride (AH). Specifically, we achieved fast (4–6 min) on-demand dissolution via the host-guest exchange mechanism upon exposure. This is radically faster than those dissoluble hydrogels using more complex synthesis methods [11,12,18,

Table 1
Comparison of current on-demand dissoluble synthetic hydrogels developed for wound care and the SHH proposed in this study.

Types	Approach	Storage Modulus (G')	Self- Healing	Wound Type	DSA and Dissolution time	Hydrogel Toxicity	DSA Cytotoxicity	Throughput/ Scalability
CCHs	Thiol-thioester exchange [11]	10 kPa	N/A	Burn & others	CME 30 min	Insufficient in vitro data & in vivo study	Significant toxicity (only tested with fibroblasts)	Very low (8–10 steps)
	Thiol-disulfide exchange [15]	2 kPa	N/A	Nitrogen mustard injuries	GSH 30–40 min (1% GSH) 15–20 min (3% GSH) 10–15 min (5% GSH)	Insufficient <i>in vitr</i> o data & lack <i>in-vivo</i> study	Not reported, <b>likely toxic</b>	High (3 steps)
	Selenol chemistry [12]	10 kPa	N/A	N/A	H <sub>2</sub> O <sub>2,</sub> 30 min	Insufficient in-vitro, lack of in-vivo study	Not reported	High (3 steps)
PCHs	Supramolecular hydrogel [19]	1.2 kPa	1 min	N/A	MH 2 min (100 mM MH)	Insufficient <i>in vitro</i> data, lack of <i>in-vivo</i> study	Not reported, <b>likely toxic</b> due to high DSA conc (100 mM)	Very low (6 steps)
SHH (this study)	Supramolecular hybrid hydrogel	50 kPa	1 min	Target: Burn, 2nd degree	AH, MH, derivatives 4–6 min (w/ 20–40 mM AH)	No toxicity, >90% viability <i>in vitro</i> , well tolerated <i>in vivo</i>	No toxicity on human keratinocytes & fibroblasts	Very high (2 steps)

CME: L-cysteine methyl ester, GSH: Glutathione, MH: Memantine hydrochloride, AH: Adamantine hydrochloride.

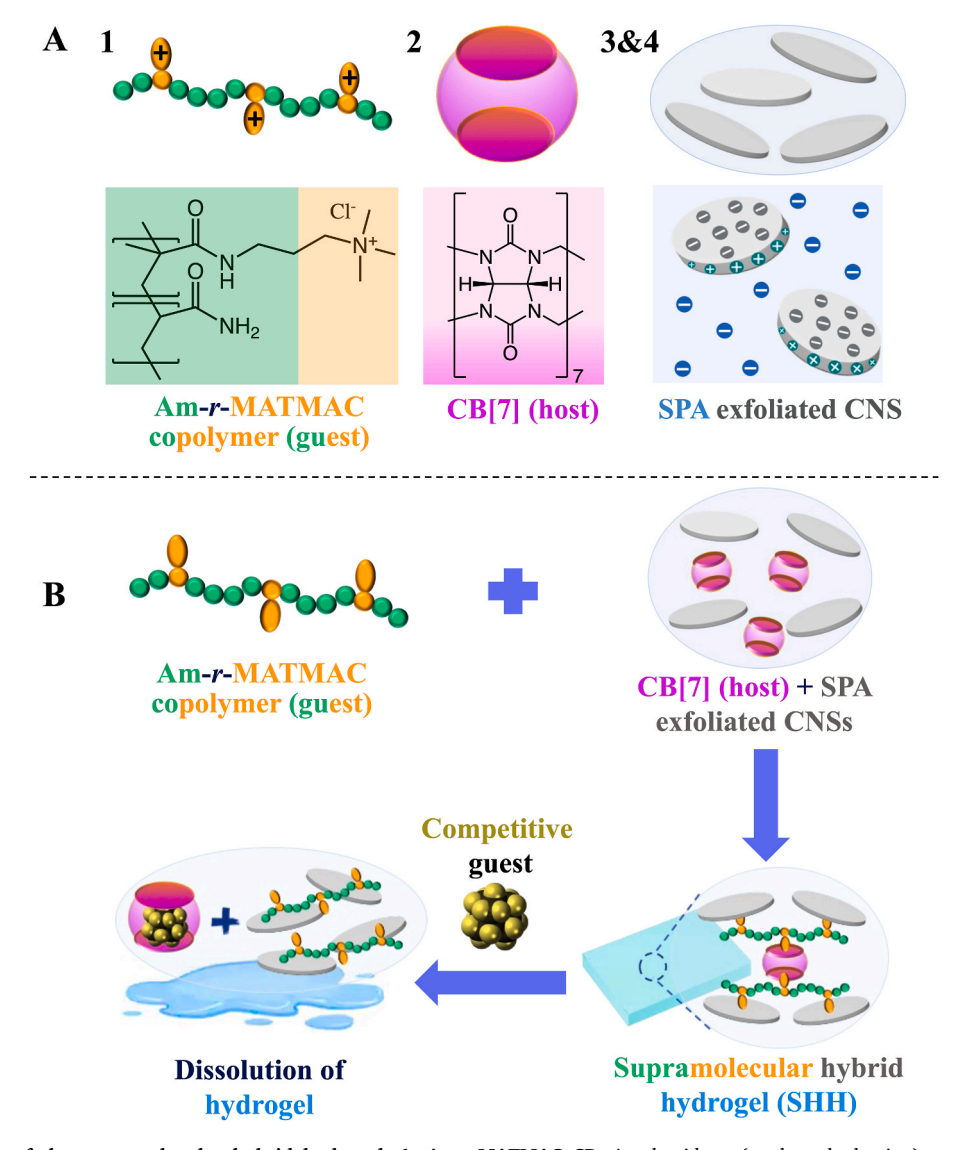


Fig. 1. A) Components of the supramolecular hybrid hydrogel. 1. Am-r-MATMAC CP: Acrylamide-co-(methacryloylamino) propyl] trimethylammonium chloride copolymer; 2. CB[7]: Cucurbit[7]uril, 3&4. CNS: Clay nanosheets and SPA: Sodium polyacrylate. The cationic edges of the aggregated CNS interacts with anionic SPA; thus, CNS is dispersed in water, B) Synthesis, formation, and on-demand dissolution of supramolecular hybrid hydrogels.

19]. These SHHs can autonomously self-heal in 1 min through the reversible host-guest interactions, which is critical for improving the lifetime and performance of hydrogels in the clinic. We also evaluated the cytotoxicity of the SHHs both in vitro and in vivo, crucial for clinical translation. In vitro cytotoxicity tests showed that SHHs and the dissolution agent amantadine hydrochloride (AH) did not have any adverse effects on human dermal fibroblasts (HDF) and human epidermal keratinocytes (HEK). Similarly, the cytokine response to the SHHs was minimal (comparable to the negative control group), indicating that the SHHs did not activate HDF and HEK in vitro. In vivo histology and immunofluorescence staining data in mice concluded that no immune and inflammatory cells populated in the subcutaneous tissue and circulating cytokines (interleukin (IL-6), granulocyte 6 colony-stimulating factor (G-CSF), keratinocyte chemoattractant (KC)) in blood showed similar levels with the sham group.

Our results demonstrate that these novel SHHs are mechanically tough, rapidly on-demand dissoluble, self-healable, and biocompatible. The novelty of our synthesis method lies in its radical simplicity (two steps), speed (<1 min), and scalability during both manufacture and use, which distinguishes our approach from existing methods. Therefore, this method promises a straightforward, rapid, and cost-effective approach

for engineering clinical dressings for burn wound healing applications.

# 2. Experimental section

# 2.1. SHH synthesis and characterization

# 2.1.1. Chemicals

Acrylamide (Am), [3-(Methacryloylamino) propyl] trimethylammonium chloride solution, 50 wt % in H<sub>2</sub>O (MATMAC), cucurbit[7]uril hydrate (CB[7]), sodium polyacrylate (SPA), amantadine hydrochloride (AH), memantine hydrochloride (MH), and N, N, N', N'-Tetramethyl ethylenediamine (TEMED), lipopolysaccharides from Escherichia coli O111:B4- LPS (LPSs), citrate buffer (pH 6), Tris-EDTA buffer (pH 8) were all purchased from Sigma Aldrich (St. Louis, MO). Laponite XLG-XR (clay nanosheets) was acquired from Acme-Hardesty Co. (Blue Pell, PA). Sodium bicarbonate buffer (pH 10) was purchased from Bioworld (Dublin, OH). Acetate buffer, reagent alcohol, acetonitrile (ACN) and ammonium persulfate (AMPS), Live/Dead Cell Viability/Cytotoxicity Kit, and presto blue were obtained from Thermo Fisher Scientific (Waltham, MA). Deuterated methanol was sourced from Cambridge Isotope Laboratories Inc. (Tewksbury, MA). Hematoxylin and eosin were

purchased from Leica Biosystems (Germany). All chemicals and solvents were of reagent grade and used as received.

# 2.1.2. Synthesis and characterization of the copolymer

random copolymer poly(acrylamide-random-(3-methacryloylamino) propyl trimethylammonium chloride) (Am-r-MATMAC) was synthesized following a free radical polymerization (Fig. S1A). Briefly, 6 mL MATMAC and 7 g Am were dissolved in 100 mL distilled water in a 250 mL round bottom flask at room temperature. 0.1 g of the initiator AMPS was added after dissolution. The reaction mixture was purged with nitrogen for 15 min. Then, 0.067 mL TEMED in 0.5 mL water was added into the mixture dropwise with a syringe. After 15 min nitrogen purge, the reaction was conducted by stirring at 250 rpm for an hour at room temperature (25  $^{\circ}$ C). Then, the reaction mixture was poured into a 1:1 mixture of ACN and reagent alcohol to precipitate out the copolymer and followed by three successive washes to eliminate any remaining unreacted monomer. The attained solid polymer was dried for two days under a fume hood and two more days in a vacuum oven at 50 °C. The product yield was 75% and calculated from the ratio of the mass of the product copolymer to the mass of the monomers used. The chemical composition of the copolymer was obtained by <sup>1</sup>H NMR (Bruker Avance III 500 MHz spectrometer, DMSO-d6). The binding interaction between the host (CB[7]) and the guest (Am-r-MATMAC) was also confirmed by <sup>1</sup>H NMR in a neutral D<sub>2</sub>O solution using different CB[7] and MATMAC ratios.

# 2.1.3. Synthesis of SHHs

For SHH-4 synthesis, SPA (4.2 mg) was added to a stirred suspension of CNSs (60 mg) in water (3 mL). After 15 min, the addition of SPA stabilized the exfoliation of CNSs. Then, CB[7] (8 mg) was added to this mixture, and the mixture was vortexed to achieve complete dissolution. Finally, Am-r-MATMAC copolymer (CP) (7.3 mg) was added, and the mixture became completely stiff within only 15 s, forming a hydrogel. As a control, we performed the same protocol with only SPA (1.8 mg), CNSs (60 mg), and CB[7] (8 mg) without the Am-r-MATMAC copolymer. Different concentrations of CNS, CB[7], SPA and CP were also tested to assess hydrogels' mechanical properties. Selected hydrogel (SHH-4) was tested for dissolution kinetics (Table 1).

# 2.1.4. Rheological tests

The rheological properties of SHHs were measured at 25 °C using a rheometer (TA Instruments, Discovery HR 20 Rheometer, New Castle, DE) fitted with parallel plates (diameter 20 mm). The gap at the apex of the para-plate was set to be 2 mm. The samples (8 mm dia.,  $\approx$  2 mm thickness) were placed between the para-plate and the platform with special care to avoid water evaporation. Dynamic frequency sweep tests (0.1-80 rad/s) at a fixed strain ( $\gamma$ ) of 0.5% were measured to determine the storage modulus (G') and loss modulus (G") of hydrogels. Three batches of SHHs (N = 3) were tested for rheological tests. To investigate the self-healing properties of hydrogels, oscillatory strain sweep measurements were performed (frequency,  $\omega = 6.0 \text{ rad/s} (1.0 \text{ Hz})$ ) to determine the collapse of the SHH from a gel state to a quasi-liquid state. Then, step-rate time-sweep measurements were performed using the following procedure: frequency,  $\omega = 6.0 \text{ rad/s} (1.0 \text{ Hz})$ , SHH-4 was subjected to 0.1% strain for 300 s, then 600% strain was applied to damage the hydrogel for 150 s and later strain went back to 0.1% for recovery for another 300 s. This continuous measurement was repeated three times. Three batches of SHHs (N = 3) were tested for each rheological test.

# 2.1.5. Compression tests

Mechanical properties (Young's modulus) were analyzed using TA Instruments RSAIII Dynamic Mechanical Analyzer (DMA) (Rheometrics Solids Analyzer). SHHs, 8 mm in diameter, were prepared for compression testing. The linear behavior in the stress-strain curve at strain levels below 1% is allowed using Hooke's law ( $E = \sigma/\epsilon$ , where  $\sigma$  is

the applied stress and  $\boldsymbol{\epsilon}$  is the resultant strain) to calculate Young's modulus.

#### 2.1.6. On-demand dissolution

We prepared different concentrations of high binding constant guests (20, 40 mM) to observe the dissolution kinetics. Amantadine hydrochloride (AH) was used as the competitive guest. i.e., the dissolution agent (DSA). In addition, SHHs ( $2\times1~cm^2$ , 2 mm thickness) were prepared, and rhodamine B and methylene blue dye was added during gelation for visualization. Finally, gauze soaked in different aqueous concentrations of selected DSA solutions (20 mM AH (0.075 g) and 40 mM AH (0.15 g)) in culture media (20 mL) was administered to the hydrogel (SHH-4), and time was recorded until complete dissolution was achieved.

## 2.1.7. Self-healing ability

Two SHHs (SHH-4) were prepared in a flower-shaped mold and stained with either rhodamine B (pink) or methylene blue. Then, they were cut into two equal parts. Two halves of alternate-colored hydrogels were combined to form color blended (pink and blue) flower-shaped SHHs at 25  $^{\circ}\text{C}$  without any external intervention. Self-healing was affirmed by the ability of the repaired flower-shaped hydrogel to retain its structure when hanging under gravity. Three batches of SHHs (N = 3) were tested for self-healing experiments.

# 2.1.8. pH stability and swelling ratio

We prepared SHHs (SHH-4) to test the pH stability and swelling ability of hybrid hydrogels. For pH stability, SHHs were synthesized in glass bottles. After gelation was completed, 5 mL of acetate buffer (pH 5), citrate buffer (pH 6), PBS buffer (pH 7.4), tris-EDTA buffer (pH 8), sodium bicarbonate buffer (pH 10, 1 M) were added into each bottle, and SHHs allowed to stand at room temperature for 72 h.

Swelling measurements were performed gravimetrically. The SHHs (SHH-4, 4 mm dia., 4 mm thickness) were dried in an oven at 60  $^{\circ}\text{C}$  for an hour. Then dried SHHs with known weights were immersed in the PBS at 37  $^{\circ}\text{C}$ . The swellen samples were taken out and weighted at predetermined time intervals. The swelling ratio was determined using the following equation:

Swelling ratio (%) =  $W_s/W_i * 100$ 

where W<sub>s</sub> and W<sub>i</sub> were the weights of hydrogels at the swelling state and the initial state, respectively [18].

Three batches of SHHs (N = 3) were tested for both pH stability and swelling measurements.

#### 2.2. In vitro biocompatibility of SHHs

# 2.2.1. Cell lines and culture

Cryopreserved human dermal fibroblasts (HDF) were obtained from Cell Applications (San Diego, CA) and culture in fibroblast growth medium (Sigma Aldrich (St. Louis, MO)). Primary human epidermal keratinocytes (HEK), keratinocyte growth kit, dermal cell basal medium, and phenol red were purchased from ATCC (Manassas, VA). Epidermal cells' media were supplemented with 1% penicillin-streptomycin solution (ATCC, Manassas, VA). HDF and HEK were cultured and passaged according to the protocols provided by the manufacturer.

2.2.2 SHHs toxicity: HDF and HEK were seeded into 24 well plates with an initial density of 10000 cells per well. The cells were incubated for 48 h in their respective culture media to allow attachment and reach confluency before the toxicity experiments. Then, the media in each well was removed, and the cells were rinsed with PBS. SHHs (8 mm dia.  $\approx 1$  mm thickness) were suspended in sterile PBS for two days and then were added into the wells, where they were incubated with the different cells (n = 4, for each group) for another 24 h. Control groups were incubated without SHHs. The cell viability was assessed by a) live/dead cell

viability/cytotoxicity staining kit and b) by presto blue assay to quantify the percentage of living cells compared to the controls. For staining, 1:250 calcein AM and 1:25 ethidium homodimer-1 combined and vortexed in PBS and 0.5 mL solution/well were added, and cells were incubated for 20 min at 37 °C. After PBS rinsing, the fluorescent images were captured using the Evos FL imaging system (Thermo Fisher Scientific, Waltham, MA). For quantitative analysis, presto blue was added (10% v/v) directly into cell culture media in each well (n = 4, for each group) with and without SHHs hydrogel. After an hour of incubation, 100  $\mu$ L of culture supernatants were collected, and the absorbance was measured in a plate reader at 570 nm and 600 nm. The percentage of living cells was normalized to controls.

## 2.2.2. Dissolution agent toxicity

HDF and HEK were cultured in 96 well plates with an initial density of 1000 cells per well. After rinsing the cells with PBS, 0.1 mL of amantadine hydrochloride (AH) (2 (0.0075 g), 10 (0.0375 g), 20 (0.0750 g), 40 (0.15 g) mM in 20 mL cell culture media) and memantine hydrochloride (MH) (2 (0.0071 g), 10 (0.035 g), 20 (0.071 g) mM) solution were added into each well. After AH and MH treatment (6 min with 2, 10, 20 mM, and 4 min with 40 mM and 60 mM), live/dead cell viability staining and presto blue assay were performed as described above.

# 2.2.3. Quantification of cytokines

We collected culture supernatants of HDF and HEK after exposing cells to SHHs for 24 h. Cell culture and LPS-supplemented media (10 ng/ mL for HDF 100 ng/mL for HEK) were utilized as negative and positive controls, respectively (n = 3 for each positive and negative controls, n =4 for SHHs treated groups). The levels of cytokines, chemokines, and growth factors were quantified using a Human High Sensitivity T-Cell Discovery Array 48-plex (HDHSTC48) (Eve Technologies, Calgary, AB, Canada). The multiplexing analysis was performed using the Luminex<sup>TM</sup> 200 system (Luminex, Austin, TX, USA). Forty-eight markers were simultaneously measured in the samples using Human Cytokine 48-Plex Discovery Assay® (MilliporeSigma, Burlington, Massachusetts, USA) according to the manufacturer's protocol. The 48-plex consisted of soluble CD40 ligand (sCD40L), epidermal growth factor (EGF), Eotaxin, fibroblast growth factor (FGF-2), Fms-like tyrosine kinase receptor 3 ligand (FLT-3 ligand), fractalkine, granulocyte colony stimulating factor (G-CSF), granulocyte macrophage-colony stimulating factor (GM-CSF), growth-regulated oncogene  $\alpha$  (GRO $\alpha$ ), interferon alpha-2 (IFN- $\alpha$ 2), interferon gamma (IFN-γ), interleukin 1 alpha (IL-1α), interleukin 1 beta (IL-1β), interleukin 1RA (IL-1RA), interleukin 2 (IL-2), interleukin 3 (IL-3), interleukin 4 (IL-4), interleukin 5 (IL-5), interleukin 6 (IL-6), interleukin 7 (IL-7), interleukin 8 (IL-8), interleukin 9 (IL-9), interleukin 10 (IL-10), interleukin 12 p40 (IL-12 (p40)), interleukin 12 p70 (IL-12 (p70)), interleukin 13 (IL-13), interleukin 15 (IL-15), interleukin 17A (IL-17A), interleukin 17E (IL-17E)/interleukin 17F (IL-17F), interleukin 25 (IL-25), interleukin 18 (IL-18), interleukin 22 (IL-22), interleukin 27 (IL-27), interferon gamma-induced protein 10 (IP-10), monocyte chemoattractant protein-1 (MCP-1), monocyte chemoattractant protein-3 (MCP-3), macrophage colony-stimulating factor (M-CSF), macrophagederived chemokine (MDC), monokine induced by gamma interferon/ Chemokine (C-X-C motif) ligand 9 (MIG/CXCL9), macrophage inflammatory protein-1 alpha (MIP-1α), macrophage inflammatory protein-1 beta (MIP-1β), platelet-derived growth factor AA (PDGF-AA), PDGF-AB/BB, regulated upon Activation, Normal T Cell Expressed and Presumably Secreted (RANTES), Transforming growth factor  $\alpha$  (TGF- $\alpha$ ), tumor necrosis factor-alpha (TNF- $\alpha$ ), tumor necrosis factor-beta (TNF- $\beta$ ), vascular endothelial growth factor (VEGF-A). Assay sensitivities of these markers range from 0.14 to 50.78 pg/mL for the 48-plex. Individual analyte sensitivity values are available in the MILLIPLEX protocol.

#### 2.3. In vivo biocompatibility of SHHs

BALB/C mice aged 7–8 weeks, weighing 17–21 g, were used for the in-vivo biocompatibility test. The animals were supplied from Charles River Laboratories (Wilmington, MA, USA) and housed at the Center of Comparative Medicine of Massachusetts General Hospital (MGH) with access to food and water ad libitum and subjected to a 12-hr light/dark cycle at room temperature (21  $^{\circ}$ C) and relative humidity of 30–70%. All protocols were in accord with the guidelines set by the Committee on Laboratory Resources, National Institutes of Health, and reviewed and approved by the Institutional Animal Care and Use Committee (IACUC, Protocol #2015N000073) of MGH.

Groups of mice (n = 3–4) were used to evaluate biocompatibility. SHHs (8 mm diameter, 2 mm thickness) were immersed and sterilized in isopropyl alcohol and then PBS (pH 7.4) for 24 h before being subcutaneously implanted on the dorsum. As positive controls, small intestinal submucosa was used to trigger an immune response in mice [42]. As sham controls, subcutaneous pockets without SHHs were made on the dorsum. The mice were sacrificed two days after the implantation. The surrounding tissue of the implantation sites was collected and fixed for histology or homogenized for cytokine measurements. The circulating blood was drawn from the inferior vena cava for systemic cytokine measurements.

# 2.3.1. Histology analysis

The dorsal tissues -from negative and positive controls and SHHs implanted samples- were immersed in 10% formalin for 24– $48\,h$  at room temperature and then embedded in paraffin and cut into  $5\mu$  sections. The sections were stained with hematoxylin and eosin (H&E) to visualize the infiltrating immune cells surrounding the biomaterial. The stained sections were imaged using a Nikon Eclipse E800 microscope (Nikon, Melville, NY).

#### 2.3.2. Immunohistochemistry

Paraffin sections were deparaffinized in xylene and rehydrated in 100%, 95%, and 70% ethanol. Antigen retrieval was performed using the Declokar chamber (Biocare Medical, Concord, CA) in Declokar buffer according to the manufacturer's instructions. The sections were then blocked with 10% goat serum, followed by incubation with primary antibodies targeting CD45 (1:40, ab10558, Abcam) or CD68 (1:100, ab125212, Abcam) at 4 °C overnight. The sections were then incubated with Alexa Flour 555 secondary antibody (1:200, ab150078, Abcam). Finally, the sections were coverslipped using an antifade mounting medium containing 4, 6-diamidino-2-phenylidole (DAPI, H-1800, Vector Laboratories, Burlingame, CA). Images were taken and quantitated using the EVOS M5000 imaging system (Invitrogen, Bothell, WA).

# 2.3.3. Quantification of systemic cytokines

For systemic cytokines analysis, plasma-heparin was separated from blood by centrifugation. We used Luminex xMAP technology for multiplexed quantification of 32 Mouse cytokines, chemokines, and growth factors. The multiplexing analysis was performed using the Luminex<sup>TM</sup> 200 system (Luminex, Austin, TX, USA) by Eve Technologies Corp. (Calgary, Alberta). Thirty-two markers were simultaneously measured in the samples using Eve Technologies' Mouse Cytokine 32-Plex Discovery Assay® (Millipore Sigma, Burlington, Massachusetts, USA) according to the manufacturer's protocol. The 32-plex consisted of Eotaxin, granulocyte colony stimulating factor (G-CSF), granulocyte macrophage-colony stimulating factor (GM-CSF), interferon gamma (IFNγ), interleukin 1 alpha (IL-1α), interleukin 1 beta (IL-1β), interleukin 2 (IL-2), interleukin 3 (IL-3), interleukin 4 (IL-4), interleukin 5 (IL-5), interleukin 6 (IL-6), interleukin 7 (IL-7), interleukin 9 (IL-9), interleukin 10 (IL-10), interleukin 12 (IL-12 (p40)), interleukin 12 (IL-12 (p70)), interleukin 13 (IL-13), interleukin (IL-15), interleukin 17 (IL-17), interferon gamma-induced protein 10 (IP-10), keratinocytesderived chemokine (KC), leukemia inhibitory factor (LIF), LPS-induced

A.A. Gokaltun et al.

Bioactive Materials xxx (xxxx) xxx

Bioactive Materials xxx (xxxx) xxx

CXC chemokine (LIX), monocyte chemoattractant protein-1 (MCP-1), macrophage colony-stimulating factor (M-CSF), monokine induced by gamma interferon (MIG), macrophage inflammatory protein-1 alpha (MIP-1 $\alpha$ ), macrophage inflammatory protein-1 beta (MIP-1 $\beta$ ), macrophage inflammatory protein-2 (MIP-2), regulated upon activation, normal T cell expressed and presumably secreted (RANTES), tumor necrosis factor (TNF- $\alpha$ ), and vascular endothelial growth factor (VEGF). Assay sensitivities of these markers range from 0.3 to 30.6 pg/mL for the 32-plex. Individual analyte sensitivity values are available in the Millipore Sigma MILLIPLEX® MAP protocol.

# 2.4. Statistical analysis

All quantitative data were analyzed using the Origin Pro 2021 Graphing and Analysis Software v.9.0.8.200 (OriginLab, Northampton, Massachusetts). and are presented as the mean  $\pm$  standard error of the mean (SEM) from at least three hydrogels from different batches. All experiments using HDF and HEK were performed four times (experimental replicates, N = 4) and at least assessed four different wells (technical replicates, n = 4). To evaluate  $\it in vivo$  biocompatibility, a total of 14 mice were used in histology, immunostaining, and circulating cytokine analyses (n = 4 for positive controls, n = 5 for negative (sham) controls and n = 5 for SHH-4 implantation). The statistical significance of the results was assessed using one-way ANOVA. Statistical significance is defined p < 0.05 for all experiments.

# 3. Results

## 3.1. Synthesis and formation of supramolecular hybrid hydrogels (SHHs)

Supramolecular "hybrid" hydrogels (SHHs) can be formed by combining inorganic components with the host-guest chemistry of organic compounds. Our SHHs consisted of four components: 1. customdesigned cationic copolymers (CPs) of 3-[(Methacryloylamino)propyl] trimethylammonium chloride (MATMAC) with acrylamide (Am), (Amr-MATMAC) CP, (guest, cationic); 2. cucurbit[7]uril (CB[7]) molecules (host); 3. clay nanosheets (CNSs) exfoliated and stabilized with 4. sodium polyacrylate (SPA, anionic) [33,35-37,43,44] (Fig. 1A). Among the cucurbituril family, we selected CB[7] since it has particularly high water solubility, up to  $30\ mM^{27}$ , and low cytotoxicity [45]. The portals of CB[7]s are highly electronegative and make them highly attractive for cation binding through the ion-dipole effect [46]. In addition, we incorporated exfoliated CNSs in our hydrogel network since previous studies indicated that the inclusion of clay minerals led to significant improvements in the mechanical strength of resultant hydrogels [33-37, 43,44]. SPA was used to stabilize the exfoliated clay sheets [33,35–37, 43,44]. It also formed physical bonds with the CP through electrostatic interactions during the formation of the SHH.

We designed Am-r-MATMAC CP to be a water-soluble copolymer that combined hydrophilic acrylamide (Am) segments with positively charged quaternary amine MATMAC segments. Each CB[7] group binds with cationic groups of Am-r-MATMAC CP through host-guest interaction and creates supramolecular crosslinks. We performed 1H NMR analysis of CB[7]-MATMAC interactions (See Supporting Information: "Interaction of CB[7] and MATMAC" and Fig. S2). This analysis shows that at least two MATMAC molecules can strongly bind with each CB[7], indicated by peak shifts for associated protons. The interactions between CB[7] and MATMAC enable the supramolecular cross-linking of the CP. Cationic Am-r-MATMAC CPs bind with the SPA-coated clay through electrostatic interactions to form a well-dispersed, homogeneous nanocomposite that leads to enhanced mechanical properties [33,35-37,43, 44,47] (Fig. 1B). The CP also includes highly hydrophilic, biocompatible repeat units – coming from the acrylamide groups – to further improve the hydration and fluid uptake of the hydrogel. Am-r-MATMAC CP was synthesized by free radical copolymerization. The synthesized CP, Am-r-MATMAC was found to contain 46 wt% MATMAC using <sup>1</sup>H NMR

spectroscopy in DMSO-d<sub>6</sub>. The  $^1\text{H}$  NMR spectrum of the Am-r-MATMAC CP used in this study is presented in Fig. S1, along with peak assignments. Each MATMAC unit was associated with nine protons appearing around 3 ppm and 3.1 ppm (h). The peaks around 1.9 ppm (f), 3.2 ppm (g), 3.3 ppm (e) were attributed to the CH<sub>2</sub> protons from MATMAC. The peak at 1.5 ppm (a) was assigned to the CH<sub>2</sub> protons from Am polymer backbone, whereas the peak at 1.7 ppm (c) was assigned to the CH<sub>2</sub> protons from MATMAC polymer.

The SHH was synthesized simply by mixing two aqueous solutions, one containing the Am-r-MATMAC CP and the other containing CB[7] and SPA-stabilized CNS. For the dissolution of the SHH, we applied a solution containing a dissolution agent (DSA), a competitive guest for CB [7]. The DSA was chosen among solutes with very high affinities to CB [7]. When added to the medium, the DSA molecules displaced and replaced the quaternary amine groups of the CP interacting with CB[7], breaking these physical crosslinks. This resulted in the dissolution of the SHH (Fig. 1B).

# 3.2. Characterization of SHHs

#### 3.2.1. Hydrogelation and mechanical properties

We tested a range of concentrations for each component based on previous reports with clay and dendritic molecular binders [33,37], supramolecular hydrogels mediated by pseudorotaxanes [43], and clay nanosheet hydrogels with a guanidinium-attached calix[4]arene binder [44]. We chose different concentrations (wt./v %) of CNS (2, 2.5, 3, 4), CB[7] (0, 0.26, 0.52), SPA (0.06, 0.1, 0.14) and CP (0, 0.15, 0.25, 0.50) to evaluate hydrogelation (Fig. 2A–C, Fig. S3) and mechanical properties of SHHs (Fig. 2D–I, Table 2, Table S1, Figs. S4 and S5). Among all formulations, SHH-4 — with a composition of CNS/CB[7]/SPA/CP: 2/0.6./0.14/0.25 — formed a hydrogel in under 15 s (see Supporting Video 1) and exhibited the highest mechanical properties with a storage modulus of  $\sim$ 50 kPa (Table 2, Fig. 2F). This corresponds to the lower end of skin modulus measurements [48–50], and thus we expect SHH-4 to be intact in use as a wound dressing while still allowing comfortable movement for the patients.

As controls, a mixture of the CNS, SPA, and CB[7] without the Am-r-MATMAC CP (Control 1, Fig. 2A) and a mixture of CNS, SPA, and Am-r-MATMAC CP without CB[7] (Control 2, Fig. 2B) were prepared. No gelation was observed in control 1 (Fig. 2A). This result indicates that there is no interaction between clay and CB[7], which results in hydrogelation. On the other hand, Control 2 formed a hydrogel in 7 min, likely due to the electrostatic interaction between the anionic surface of CNS with amine groups of Am-r-MATMAC CPs. Nevertheless, Control 2 has a lower mechanical strength and Young's modulus than the corresponding SHH-4, which contains the Am-r-MATMAC CP, which we discuss in the following. This result indicates that Am-r-MATMAC is essential to obtain mechanically strong and elastic hydrogels.

Next, we used a rheometer to evaluate the mechanical properties of various SHHs (Fig. 2D-I, Fig. S4). The respective storage moduli (G') and loss moduli (G'') are shown for SHHs as functions of angular frequency ( $\omega = 0.1$ –80 rad/s) at a fixed strain ( $\gamma$ ) of 0.5% (Fig. 2C–H, Fig. S4). All samples had a single plateau region in their dynamic moduli. The hydrogels demonstrated elastic response as typical hydrogels, which means G' values were always larger than the G" values over the entire range of frequencies. These tests showed high SPA concentrations (0.14 wt%) are needed to obtain strong and stable SHHs. Specifically, hydrogels made with 0.14 wt% SPA (Fig. 2F, SHH-4) has better mechanical strength than those with lower concentrations in accordance with a previous report [44] (0.06 wt% and 0.1 wt%) (Fig. 2D, Fig. 4SA). Similarly, increasing CP concentration up to 0.25 wt/v % enhanced G' values of SHHs (Fig. 2F). We attribute this increase in storage modulus to the interaction of the CP's cationic groups with CB[7]s and CNSs. The higher number of cationic groups led to a higher density of physical crosslinks through host-guest and electrostatic interactions, resulting in a stronger hydrogel. Although the formulations without SPA showed a

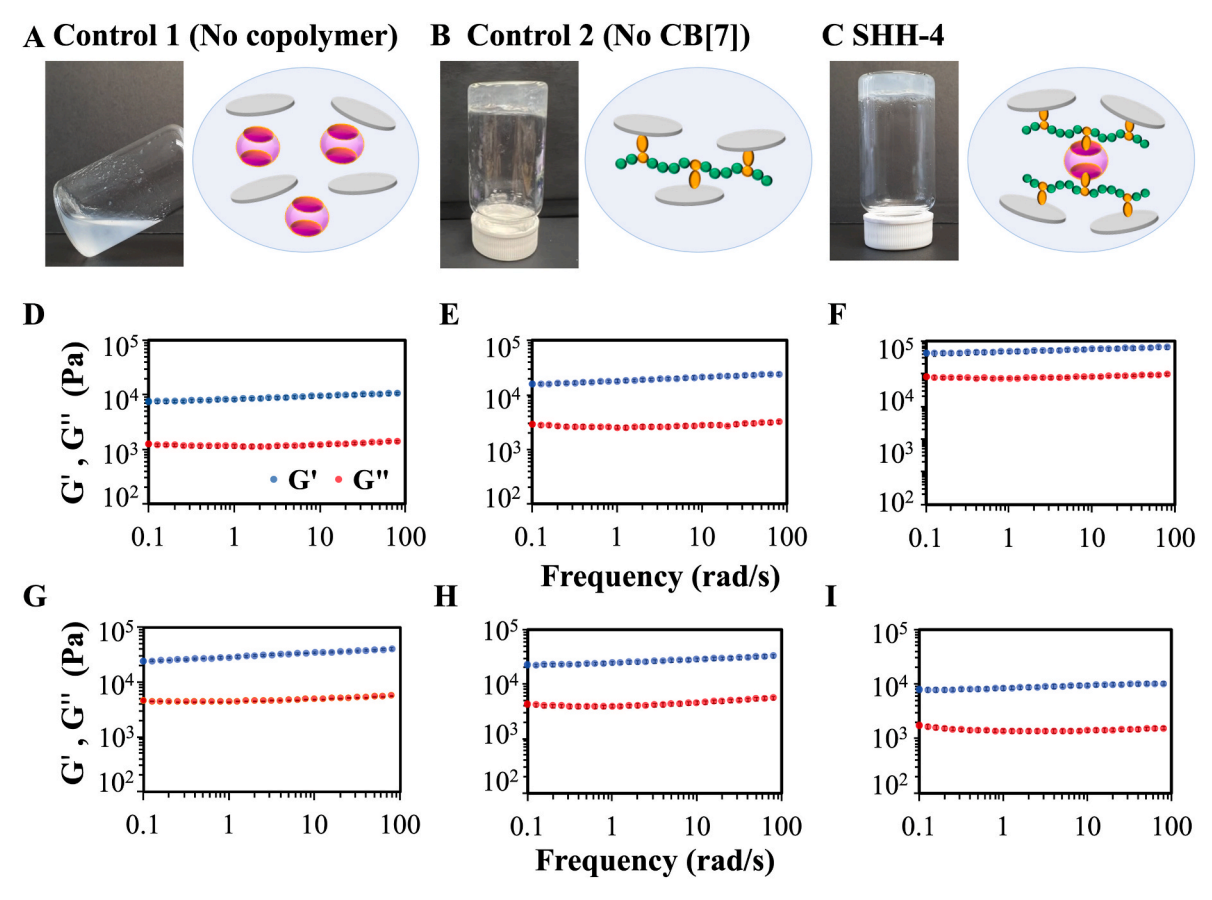


Fig. 2. Non-covalent hydrogelation and rheological properties (20 °C) of hydrogels. A) Hydrogelation of control 1. Control 1 does not contain CP, B) Hydrogelation of control 2. Control 2 does not contain CB[7], C) Hydrogelation of SHH-4. G' and G' of hydrogels at weight ratios CNS/CB[7]/SPA/CP of 2/0.26/0.06/0.15 (D, SHH-1), 2/0.26/0.14/0.15 (E, SHH-3), 2/0.26/0.14/0.25 (F, SHH-4), 2/0.26/0/0.25 (G, SHH-5), 4/0.26/0.14/0.50 (H, SHH-10), and 4/0.26/0.14/0.25 (I, SHH-12) on frequency sweep from (0.1–80 rad/s). 3 separate batches of hydrogels were synthesized (N = 3) and tested for each experiment. Data are shown as mean  $\pm$  SE (N = 3).

similar trend in mechanical strength with increasing CP concentrations (Fig. 2G, Table 2), the pretreatment of CNSs with SPA considerably increases the storage modulus by a factor of up to 2.7. This indicates that it is critical to pretreat CNSs with SPAs to obtain strong hydrogels [33,43,51]. We also tested the effect of CNS concentration on mechanical strength. We observed that the mechanical properties decreased by further increasing CNS (2.5, 3, 4 wt/v %) and CP concentration (0.50 wt %) (Fig. 2H and I, Fig. S4D-E-F). At higher CNS concentrations, we believe that the delamination of CNSs could not be effectively achieved via SPA, and as a result, electrostatic interactions between CNSs and CP decreased; thus, relatively weaker hydrogels were obtained compared to SHH-4.

We also assessed the effects of CB[7] concentration on mechanical properties. To this end, we first compared the rheological and mechanical properties of SHH-4 and SHH-4 without CB[7], i.e., Control 2 (Fig. S5, Table S1). We found that without CB[7] (Control 2), hydrogelation took over 7 min as opposed to mere 15 s with CB[7] (SHH-4). Further, the G' values of SHH-4 without CB[7] (Control 2) were approximately 15 times lower than SHH-4 (Figs. S5A and B). Moreover, oscillatory strain sweep measurements were performed to compare and identify the breakdown oscillatory force (Fig. 5C &D) of these hydrogels. SHH-4 without CB[7] (Control 2) collapsed from gel state to a quasiliquid state above the critical strain ( $\gamma$ ) of 120% (tan delta = G''/G'  $\approx$  1.3) whereas SHH-4 required 4.5 times higher oscillatory force,  $\gamma =$ 550%, (tan delta = G''/G'  $\approx$  1.4) for the breakdown. Thus, the strength of SHH-4 is attributed to the supramolecular interactions between CB[7] and Am-r-MATMAC CP, which is crucial to obtaining mechanically strong hydrogels. We also performed compression tests to calculate and

compare Young's modulus of SHH-4 and Control 2. (Table S1). Consistent with rheological properties, we observed Young's modulus of SHH-4 is three times higher than Control 2.

We observed that beyond certain concentrations, *i.e.*, those used in SHH-4, further addition of CP and CB[7], without increasing the concentration of CNS, resulted in mechanically weaker hydrogels (SHH-6 and SHH-7). We posit that these decreases are likely due to an insufficient number of CNS that can bind to the CB[7]-CP host-guest complexes, resulting in domains where CB[7]-CP complexes are free. Conversely, if we increase the CNS concentration beyond SHH-4, without changing the CB[7] and CP concentrations, we also achieve weaker gels (SHH-8, SHH-11, SHH-12), indicating that excess CNS can also form free domains. We thus posit that the ratio between all three major components – CB[7], CP, and CNS – might be ideal in SHH-4, which will require further assessment in future work with derivatives based on this ratio. Overall, we achieved the highest storage modulus (average G' = 50 kPa > G'') with SHH-4 and selected this hydrogel for further characterization and evaluation *in vitro* and *in vivo*.

# 3.2.2. On-demand dissolution

The dissolution of SHHs relies on the host-guest exchange mechanism whereby a competitive guest (DSA) displaces the existing guest molecules (CPs). Adamantane (AD) or diamantane (DA) derivatives stand out as DSA candidates due to their very high guest-binding affinities with CB[7]s<sup>28</sup> ranging from 2x10 [12] -  $7.2 \times 10^{17}$  M $^{-1}$ . This provides a large dynamic range for the choice of competitive guests [52]. Here we used amantadine hydrochloride (AH) [28] – a member of the AD family – as the competitive guest molecule (*i.e.*, DSA) for

Table 2 Compositions of supramolecular hybrid hydrogels (SHHs) 3 separate hydrogels were tested (N = 3) for each experiment. The data are shown as mean  $\pm$  SE (N = 3). Please see the statistical analyses of these measurements in Supporting Information (Fig. S6).

	CNS (wt./v) %	CB[7] (wt./v) %	SPA (wt./v) %	CP (wt./ v) %	G' <sub>(1)</sub> (Pa)	G" <sub>(2)</sub> (Pa)
Control-	2	0.26	0.14	0	N/A	N/A
Control-	2	0	0.14	0.25	$3.4 \times 10^{3}$ $\pm 556.7$	$0.6 \times 10^{3} \\ \pm 132.6$
SHH-1	2	0.26	0.06	0.15	$3.5 \times 10^{3}$ $\pm 791.4$	$0.5 \times 10^{3}$ $\pm 117.5$
SHH-2	2	0.26	0.10	0.15	$\begin{array}{l} 8.7\times10^3 \\ \pm\ 571.7 \end{array}$	$1.2\times10^3\\\pm74.9$
SHH-3	2	0.26	0.14	0.15	$19.4\times10^4\\\pm1297.7$	$\begin{array}{l} 2.7\times10^3\\ \pm\ 227.7\end{array}$
SHH-4	2	0.26	0.14	0.25	$\begin{array}{l} 5.0\times10^4 \\ \pm\ 6756.6 \end{array}$	$\begin{array}{l} 7.7\times10^3 \\ \pm\ 657.6 \end{array}$
SHH-5	2	0.26	0	0.25	$\begin{array}{l} 1.8\times10^4 \\ \pm\ 2135.5 \end{array}$	$\begin{array}{l} 3.2\times10^3\\ \pm\ 416.5\end{array}$
SHH-6	2	0.26	0.14	0.50	$\begin{array}{l} 2.7\times10^4 \\ \pm\ 3657.9 \end{array}$	$\begin{array}{l} 4.1\times10^3\\ \pm\ 550.6\end{array}$
SHH-7	2	0.52	0.14	0.50	$\begin{array}{l} 1.7\times10^3\\ \pm\ 70.9\end{array}$	$\begin{array}{l} 0.2\times10^3 \\ \pm \ 4.0 \end{array}$
SHH-8	2.5	0.26	0.14	0.25	$\begin{array}{l} 1.2\times10^4 \\ \pm\ 1768.3 \end{array}$	$\begin{aligned} 1.7\times10^3\\ \pm\ 237.7\end{aligned}$
SHH-9	3	0.26	0.14	0.50	$2.4\times10^4\\\pm1056.2$	$3.8\times10^3\\ \pm40.5$
SHH-10	4	0.26	0.14	0.50	$2.6 \times 10^4 \pm 1797.2$	$4.3 \times 10^{3} \pm 341.3$
SHH-11	3	0.26	0.14	0.25	$1.3 \times 10^4 \pm 1460.6$	$2.1\times10^3\\\pm249.5$
SHH-12	4	0.26	0.14	0.25	$\begin{aligned} 8.8 \times 10^3 \\ \pm 704.1 \end{aligned}$	$1.4\times10^3\\\pm119.5$

<sup>(1):</sup> Average G' between angular frequency of 0.1-80 rad/s.

dissolution. AH binds CB[7] more strongly than the cationic groups on the CP. We note that we have attempted to increase the concentration of the AH solution beyond 40 mM to reduce the dissolution time. Nevertheless, upon a preliminary screening of concentrations via *in vitro* viability testing, we found that AH concentrations above 40 mM can be toxic to cells in the skin niche and resulted in detachment of cells from culture surfaces (Please see section 3.3.1 for further details). Accordingly, in what follows, we demonstrate dissolution tests only with 20 and 40 mM AH concentrations.

We first tested the dissolution of SHH-4 w/o CB[7] (Control 2) using 20 mM and 40 mM AH solution (Fig. S7). We did not observe any dissolution of this gel (Control 2) even after 3 days of exposure to the AH solutions. This result indicates that CB[7] is absolutely crucial for the dissolution process. Upon addition to the SHH, AH breaks the CP – CB[7] crosslinks through the host-guest exchange mechanism. As a result, SHHs rapidly dissolved upon exposure to AH (Fig. 1B). SHH-4s were dissolved in only  $\sim$ 6 min with 20 mM AH (Fig. 3A) and in  $\sim$ 4 min with 40 mM AH (Fig. 3B). Taken together with the rheological testing results, these showed that our novel supramolecular hybrid hydrogel design can provide a mechanically tough yet quickly dissoluble dressing for easy removal and dressing changes.

# 3.2.3. Self-healing ability

Self-healing enables the spontaneous regeneration and repair of a hydrogel network through covalent or non-covalent interactions after mechanical damage. Therefore, incorporating this feature into hydrogels has gained popularity in wound treatment due to the structural stability and robustness they provide [53]. In wound dressings, self-healing improves the durability and performance of hydrogels and provides a stable connection between the wound site and the dressing

[54]. This makes self-healing hydrogels a superior choice, especially in treating wounds at or near extremities (e.g., ankle, knee, and wrists).

We assessed the self-healing capacity of SHH-4 by a macroscopic damage test using two pre-gelled flower-shaped SHHs stained blue (trypan blue) and red (rhodamine B) (Fig. 3C). We first cut both gels in half using a scalpel and then allowed contact between the two different colored halves to observe their self-healing ability. We found that the cut hydrogel pieces can rapidly – in about 1 min (1.2  $\pm$  0.1 min) – combine into flower-shaped hydrogels again without any external stimulus, and the self-healed hydrogels were strong enough to be lifted (Fig. 3C). To assess the rapid recovery of SHH-4 further, we performed step-rate timesweep measurements at a constant frequency ( $\omega = 6.0 \text{ rad/s } (1.0 \text{ Hz})$ ) (Fig. S8). SHH-4 was subjected to 0.1% strain for 300 s, then 600% strain was applied to damage the hydrogel for 150 s (quasi-liquid state, tan delta =  $G''/G' \approx 1.5$ ). However, when the applied strain was reduced to 0.1% for recovery for another 300 s, G' immediately recovered its initial value (tan delta =  $G^{"}/G" \approx 0.1$ ). The rapid self-healing ability of the SHHs likely originates from non-covalent supramolecular crosslinks between Am-r-MATMAP CP and CB[7], whereas CNSs improve their mechanical strength and stability.

Our SHHs self-heal fast compared to chemically crosslinked hydrogels [55–57] which require 30 min to 1 h to recover their initial value. Besides, our SHHs eliminate the need for reactive chemicals, toxic catalysts, or external stimuli for self-healing, which are used in dynamic covalent reactions (chemical crosslinking) [58]. On the other hand, there are several examples of supramolecular hydrogels which can recover at rates comparable to our SHHs. However, their G' value is 250 times [59] and 40 times [19] smaller than SHH-4. Accordingly, we posit that our SHHs – with their simultaneous high mechanical strength and quick self-healing ability – constitute great candidates as wound dressings compared to the existing approaches.

# 3.2.4. pH stability and degree of swelling

Hydrogels can absorb and hold the wound exudate. This facilitates the proliferation of fibroblasts and the migration of keratinocytes, both essential for the complete epithelialization of the wound [47,60]. As hydrogels swell, they can trap wound debris and bacteria in the gel matrix, potentially reducing wound bioburden. Thus, here we assessed the pH stability and swelling capacity of the SHH-4 at different pH values (Fig. S9). As a swelling medium, we utilized three buffer solutions mimicking the blister fluid since its pH changes between 5 and 10 in second-degree burns [61]: acidic (pH 5 acetate buffer), neutral (pH 7.4 phosphate buffer), and basic (pH 10 Tris EDTA buffer).

We first tested the effect of pH on the stability of SHHs. SHHs were maintained for 72 h in these acidic, neutral, and basic solutions without any disruption. Next, we tested the swelling ratio of SHHs using different pH solutions. After exposure to acidic and neutral buffers (pH 5–7.4), SHHs swelled between 160% and 200%, and swelling reached equilibrium after 72 h (Fig. S9). In basic buffers, the degree of swelling increased up to 357.1  $\pm$  66.1% at pH 8 and 722.8  $\pm$  288.7% at pH 10 (Fig. S9) after 72 h.

# 3.3. In vitro biocompatibility

# 3.3.1. In vitro cytotoxicity of dissolution agents (DSAs) and SHHs

While designing an on-demand dissoluble dressing, it is critical to evaluate the DSA toxicity. We, thus, assessed dissolution agent (DSAs) toxicity on two relevant human skin cell types, *i.e.*, human dermal fibroblasts (HDF) and human epidermal keratinocytes (HEK). We exposed monolayer cultures of both cell types to solutions of amantadine hydrochloride (AH) and memantine hydrochloride with different concentrations (2–60 mM) for 4–10 min. We then assessed the cell viability via i) live/dead staining and ii) presto blue metabolic assay. The results are presented (Fig. 4) compared to control groups which were only exposed to the respective culture medium of either cell type.

Both HDF and HEK showed high viability (>90%) in AH

<sup>(2):</sup> Average G" between angular frequency of 0.1-80 rad/s.

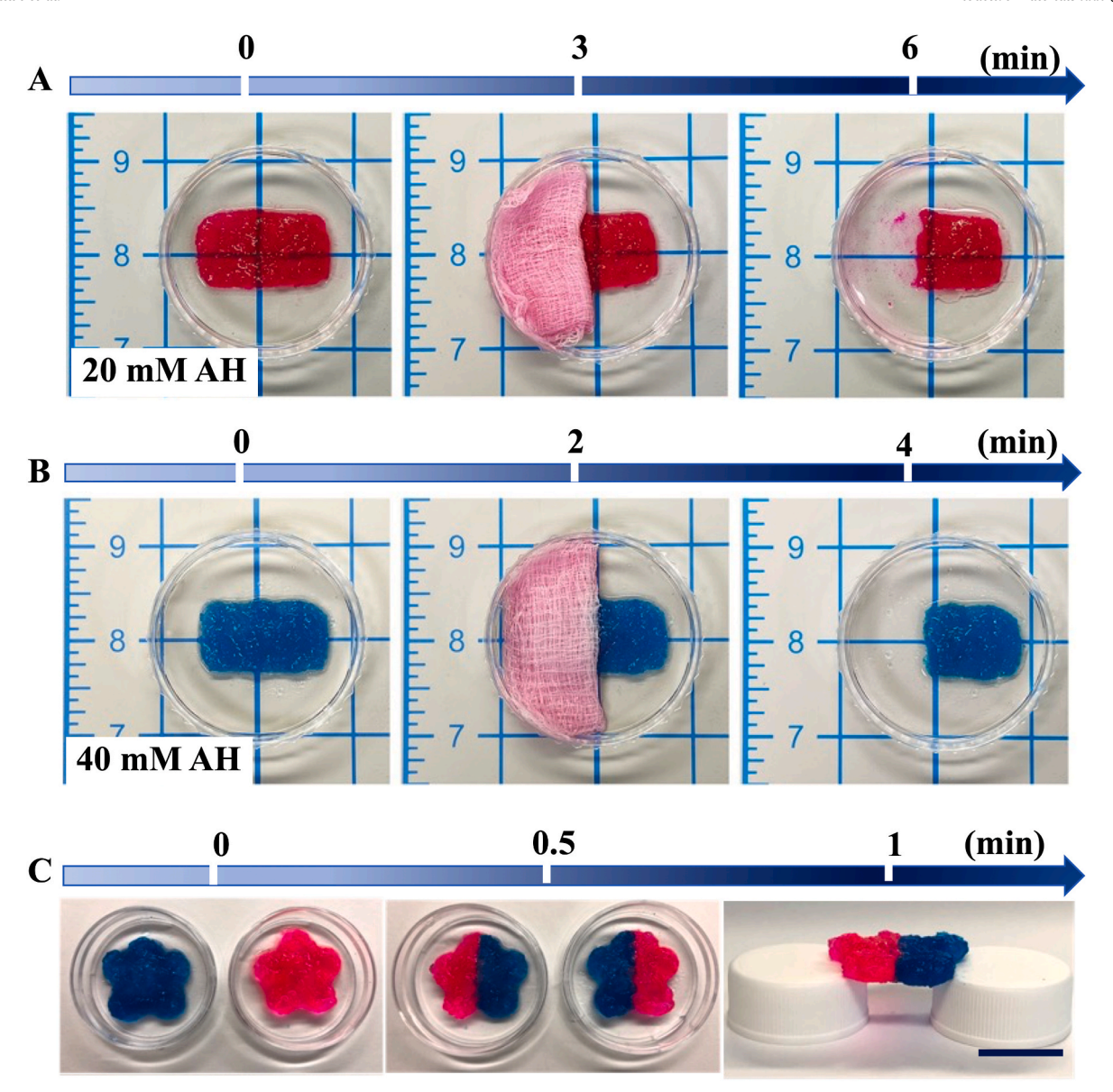


Fig. 3. On-demand dissolution and self-healing of the SHH-4. A) 20 mM and B) 40 mM AH soaked gauzes were administered to approximately one-third of the hydrogels. Rhodamine B (A) and methylene blue (B) dye were added to the hydrogel for visualization. Complete hydrogel dissolution was achieved in 6 and 4 min with 20 mM and 40 mM AH-soaked gauze, respectively. The thickness of SHHs: 2 mm. Scale bar: 1.5 cm, C) Two flower-shaped SHHs were cut and spliced. Hybrid hydrogels self-healed in 1 min without any external force. The thickness of SHHs: 4 mm, Scale bar: 1.5 cm. 3 separate batches of hydrogels were synthesized (N = 3) and tested for each experiment.

concentrations of 2-40 mM (Fig. 4A-D, Figs. S9A-B). Our results indicate that AH presents minimal adverse effects up to 40 mM on these dermal and epidermal cells. Nevertheless, a 60 mM AH concentration is toxic to the cells and results in the detachment of cells from the culture surfaces (Fig. S10A and Fig. S10B). HDF and HEK also showed high viability after exposure to 2 mM and 10 mM MH solutions, i.e., an alternative dissolution agent. However, when we increased the MH concentration to 20 mM, the viability of these cells decreased to 44  $\pm$ 7.6% (Figs. S10C-F), and some of the cells detached from the surface of the wells (Figs. S10C and D). These results indicated that MH solution can present significant toxicity to skin cells at higher concentrations. We note that the exposure scenario we tested in these in vitro experiments is extreme. In clinical applications, cells will likely not be directly exposed to the dissolution agent until the end stages of the dissolution, and the concentrations of such exposure will likely be reduced compared to the starting concentrations that we use here. These in vitro results posit that AH could constitute an ideal dissolution agent with minimal adverse

effects in further testing and clinical use.

To ensure the use of the SHHs as potential burn dressings, we tested *in vitro* cytotoxicity of the SHH-4 hydrogel with both HDF and HEK. SHH disks (4 mm diameter, 2 mm thickness) were introduced into the culture and incubated for 24 h. We then assessed the cell viability via i) live/dead staining and ii) presto blue metabolic assay. The results are presented (Fig. 5) in comparison to control groups (culture media). The viability of HDF (98.5  $\pm$  4.2%) and HEK (94.3  $\pm$  1.4%) exposed to the SHH did not differ from controls (100  $\pm$  5%) after 24 h (Fig. 5C). The introduction of SHHs led to no visible or significant differences in cell viability or morphology.

# 3.3.2. In vitro cytokine secretion of SHHs

Cytokines are soluble extracellular proteins or glycoproteins that facilitate cell-cell communication and activation of the immune and inflammatory system [62]. A design criterion for our SHHs is not to elicit any immune or inflammatory response beyond normal wound healing.

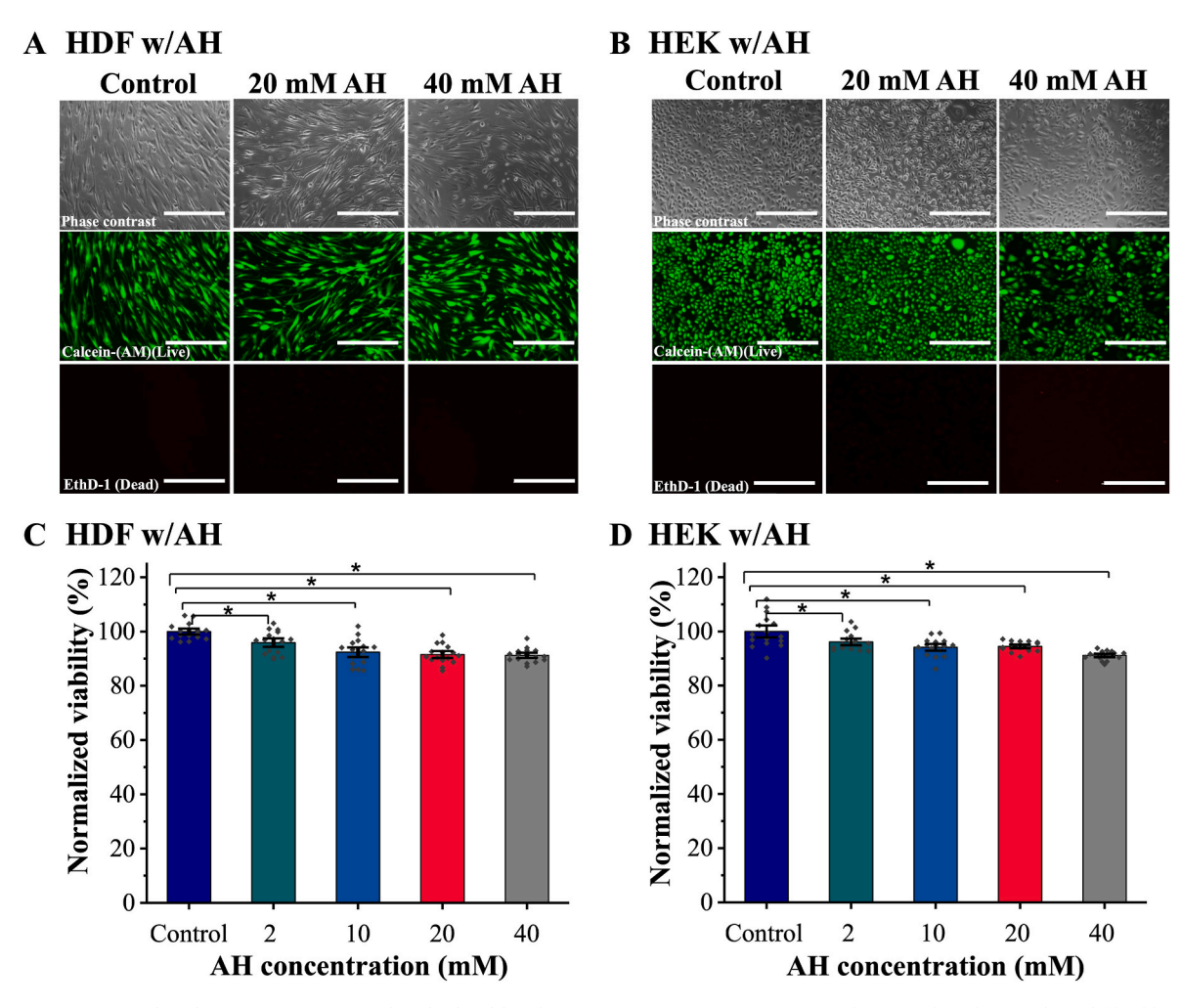


Fig. 4. *In vitro* toxicity of dissolution agent (amantadine hydrochloride (AH)) *In vitro* cytotoxicity of AH solution with A) human dermal fibroblasts (HDF), B) human epidermal keratinocytes (HEK). We treated cells with AH for 10 min (2 & 10 mM), 6 min (20 mM), and 4 min (40 mM). We used culture media for controls. Presto blue assay of AH exposed C) HDF and D) HEK. Dermal and epidermal cells treated with 2, 10, 20 mM AH solutions showed higher viability close to that of the untreated control. Higher yet minimal adverse effect was observed with 40 mM AH solution. Image scale bar: 400  $\mu$ m. Data are expressed as the mean  $\pm$  SD (n = 4, N = 4), \*  $\leq$  0.05.

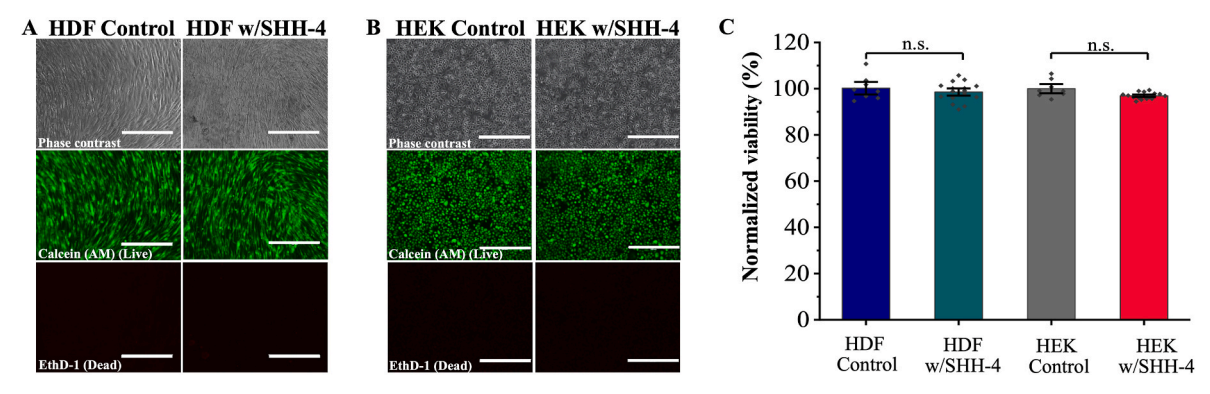


Fig. 5. In vitro toxicity of supramolecular hybrid hydrogels (SHH-4). In-vitro cytotoxicity of SHH-4 with A) human dermal fibroblasts (HDF), B) human epidermal keratinocytes (HEK) after 24 h incubation. C) Presto blue assay of SHH-4 exposed HDF and HEK. We used cells w/o SHH-4 for controls. SHH-4 exposed cells did not differ from untreated control. Image scale bar: 400  $\mu$ m. Data are expressed as the mean  $\pm$  SD (n = 4, N = 4), \*: p  $\leq$  0.05, n.s: non-significant.

Thus, as a preliminary approach, we assessed the relative secretion levels of cytokine and growth factors of *in vitro* HDF and HEK cells in response to SHH-4 (Fig. 6A–C). We profiled a panel of 48 cytokines and growth factors but only presented those where the positive control (Lipopolysaccharide, LPS) elicited a substantial regulation. Importantly, we observed that the expression of various inflammatory cytokines

growth-regulated oncogene)-alpha (GRO- $\alpha$ ), Regulated on Activation Normal T Expressed and Secreted (RANTES), Interleukin-6 (IL-6), Monocyte chemoattractant protein-1 (MCP-1), Tumour Necrosis Factor alpha (TNF- $\alpha$ ), Tumour Necrosis Factor beta (TNF- $\beta$ ) for HDF, and Granulocyte-macrophage colony-stimulating factor (GM-CSF), Macrophage colony-stimulating factor (M-CSF), Vascular endothelial growth

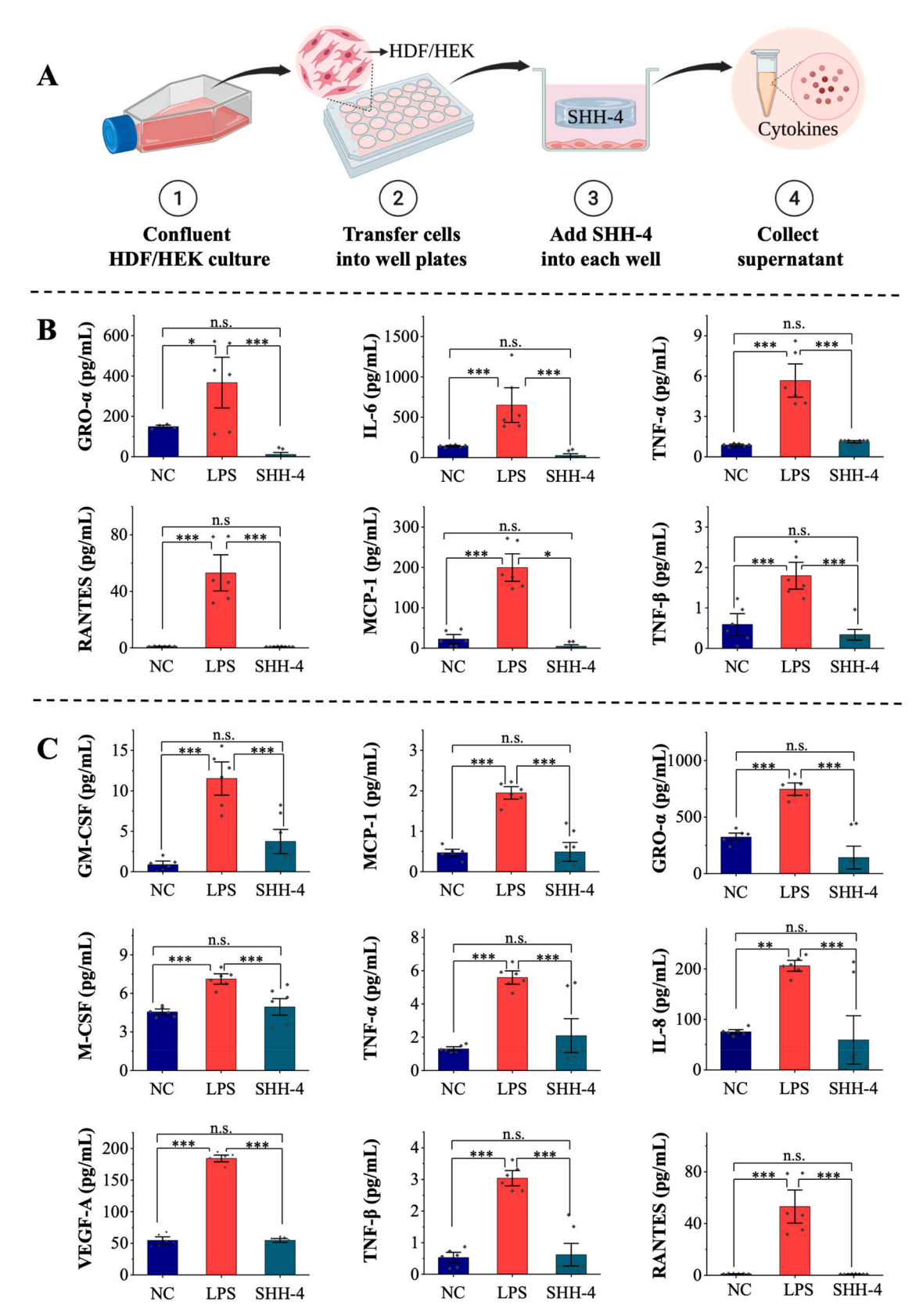


Fig. 6. In vitro cytokine expression of HDF and HEK after 24 h incubation with SHH-4. A) Schematic diagram of the procedure description, cytokine expression of B) HDF and C) HEK after SHH-4 exposure. We used LPS administration (10 ng/mL for HDF and 100 ng/mL for HEK) as positive controls. The HDF and HEK cultured without the gel were used as negative controls. Data are expressed as mean  $\pm$  SD (n = 4, N = 4). We use \*: p  $\leq$  0.05, \*\*: p  $\leq$  0.01, \*\*\*: p  $\leq$  0.001 by Tukeytest for significance comparisons between cytokine levels in the controls and SHH-4-treated groups. Cells incubated with SHH-4 did not differ from media-only controls (NC) and were significantly lower than the positive control (LPS). Fig. 6A was created with BioRender.com.

A.A. Gokaltun et al.

Bioactive Materials xxx (xxxx) xxx

Bioactive Materials xxx (xxxx) xxx

factor A (VEGF-A), Monocyte chemoattractant protein-1 (MCP-1), TNF- $\alpha$ , TNF- $\beta$ , GRO- $\alpha$ , Interleukin-8 (IL-8), RANTES for HEK did not differ from media only controls and was significantly lower than the positive controls exposed to lipopolysaccharide (LPS) (Fig. 6B and C). This lack of cytokine secretion regulation in the presence of SHHs demonstrated that HDF and HEK are not activated by the SHHs in our *in vitro* experiments.

#### 3.4. In vivo biocompatibility

The biocompatibility of the hydrogel with the skin tissue or other tissues it is intended for is essential for efficient and timely wound healing. A biocompatible hydrogel should integrate itself on the tissue with limited inflammatory response beyond normal wound healing, preferably without "foreign body reactions" such as accumulating giant cells, macrophages, and leukocytes. Moreover, it should provide healing with minimal to no fibrosis [63-65]. To assess the in vivo biocompatibility of our best-performing SHH, we subcutaneously implanted the SHH-4 hybrid hydrogels (8 mm diameter, 2 mm thickness) into the dorsal subcutaneous pockets of mice. Negative control (NC; sham, no implantation) and positive control (PC); small intestinal submucosa implantation to the dorsal pocket) experiments were also conducted simultaneously. 48 h after implantation, the surrounding tissue of the implantation site was collected for histological and immunostaining analyses, and blood was drawn from the inferior vena cava for systemic cytokine analysis (Fig. 7A).

#### 3.4.1. Histological analysis

Histological analyses were performed to evaluate the morphology and immune cell infiltration under the subcutaneous tissue. In the PC group, immune cells infiltrated the interstitial area and muscular tissues around the implants, as indicated with a dashed rectangle (Fig. 7B). In stark contrast to this drastic infiltration in the PC group, the SHH-4 group showed limited infiltration at levels similar to the sham (NC) group. These results indicate that SHH-4 implantation did not invoke any infiltration of immune cells under the subcutaneous tissue compared to the sham control (Fig. 7B).

# 3.4.2. Immunofluorescence staining

Immunohistochemistry was performed to assess the infiltration of different immune and inflammatory cells in the subcutaneous tissue and hydrogel, including general leukocytes (CD45) and macrophages (CD68) (Fig. 7C and D). CD45-positive leukocytes (including neutrophils) are immune cells which infiltrate and participate in the immune rejection and implantation failures of skin xenografts [66] and allografts [67]. CD68-positive macrophages have also been reported in the rejection of skin grafts [68], and they are often considered a therapeutic target to promote the survival of transplanted organs due to their destructive effect on the graft tissue [69]. In the sham group, no CD45 and CD68 positive immune cells were observed in the surrounding tissue of the subcutaneous pocket (Fig. 7C and D). We note that the anti-CD68 antibodies also label muscular tissue, but this labeling was excluded from the analysis based on the distinct morphology of the macrophages. High numbers of CD45 and CD68 positive cells were identified in the interstitial area around the implants in the PC group. In contrast, only a few CD45 and CD68 positive immune cells were observed around the SHH-4 implants indicating limited leukocyte and macrophage infiltration. These results are in good agreement with the H&E stained sections. We, thus, conclude that the SHH-4 implants do not trigger any significant immune responses histologically (levels are similar to the sham group and significantly lower than the PC group).

# 3.4.3. Systemic cytokine analysis

In addition to histological and immunostaining analyses, we quantified the cytokine levels in the circulating plasma to evaluate whether the implantation of SHH-4 results in any alterations in systemic cytokine

levels (Fig. 7E). We profiled a panel of 48 cytokines and growth factors but only present those where the PC elicited a substantial regulation. Among the 48 cytokines profiled, the PC group mice showed elevated levels of interleukin 6 (IL-6), granulocyte colony-stimulating factor (G-CSF), and keratinocyte chemoattractant (KC) compared to sham control and SHH-4 implants. The elevated expression of cytokines IL-6, G-CSF, and KC in the PC group are associated with immune rejection by the skin tissue. IL-6 is synthesized at the local lesion to initiate inflammation [52] and is elevated to modulate inflammatory rejection and dermal fibroblast activity in response to xenobiotic materials, such as breast silicone implants both in vitro and in vivo [70]. G-CSF is known for its regulatory role in promoting survival, proliferation, differentiation, and function of neutrophils while affecting T cell and dendritic cell functions [71,72]. The elevation of G-CSF level correlated with highly mobilized neutrophil activities around the implant of the PC group (Fig. 7B). KC (or CXCL-1 in humans), is a mediator for immune response and a potent attractant for neutrophils and other non-hematopoietic cells to the injury or infection site [73], the overexpression of KC has been found to promote higher and prolonged immune cell influx in the foreign body reaction of implanted materials in the skin tissue [74]. The low levels of these cytokines in the SHH-4 group indicated a limited activation of the neutrophils and fibroblasts comparable to the sham group and significantly lower than the positive group. This indicates that SHH-4 does not elicit any considerable immune responses beyond what is necessary for normal wound healing response (i.e., the response of the sham group). As with the local H&E and immunostaining analyses, the systemic expression of these cytokines was significantly lower in the SHH-4 implanted mice compared to the PC group and comparable to the expression in that of the sham group. We thus conclude that the SHH-4 did not elicit a significant systemic cytokine response in mice upon implantation.

# 4. Conclusion and future outlook

We created a simple, quick, and scalable method to synthesize a supramolecular hybrid hydrogel (SHH) via the supramolecular assembly of Am-r-MATMAC CP with CB[7] hosts and CNSs. Our SHH design and synthesis feature green chemistry - whereby we eliminated many toxic and reactive chemicals commonly used in traditional approaches which also results in rapid hydrogel formation ( $\sim 15$  s to gelation). As such, these SHHs are the first of their kind as burn dressings, and drastically differ from the existing lengthy and potentially hazardous methods of hydrogel preparation. Furthermore, the host-guest exchange mechanism between the Am-r-MATMAC CP and CB[7] in the SHHs, enables rapid on-demand dissolution (4-6 min) of the hybrid hydrogels. This dissolution is facilitated by the introduction of a competitive guest, AH (20 & 40 mM), without any significant adverse effects on either dermal and or epidermal cells in vitro (cell viability >90%) and in-vivo. Supramolecular crosslinks with CNSs provided distinctive functions of high mechanical strength (G' > 50 kPa; G' > G'') and fast self-healing capability (1 min) for SHH-4. In addition, SHH-4 showed high biocompatibility in vitro and in vivo. In vitro immunogenicity assessment showed a lower immune response to SHHs compared to positive (LPS) controls. Moreover, after subcutaneous hydrogel implantation in mice, in vivo histology, immunofluorescence, and systemic cytokine analyses indicated no immune and inflammatory responses beyond sham controls. As such, we posit that SHH-4 is a promising alternative to commercial hydrogels currently used in clinical burn wound treatment.

Due to the ease of their fabrication, which only involves two steps of mixing, we expect these novel SHHs will enable large-scale yet low-cost fabrication, addressing a critical bottleneck for translation to clinical applications. Further, due to this ease and the speed (15 s) of SHH formation, we envision that the dressings could even be formed at the bedside and on-field synthesis of the patients with customizations as necessary. Such novel and on-demand dissoluble SHHs have great potential as second-degree burn dressings. We expect SHH-based dressings

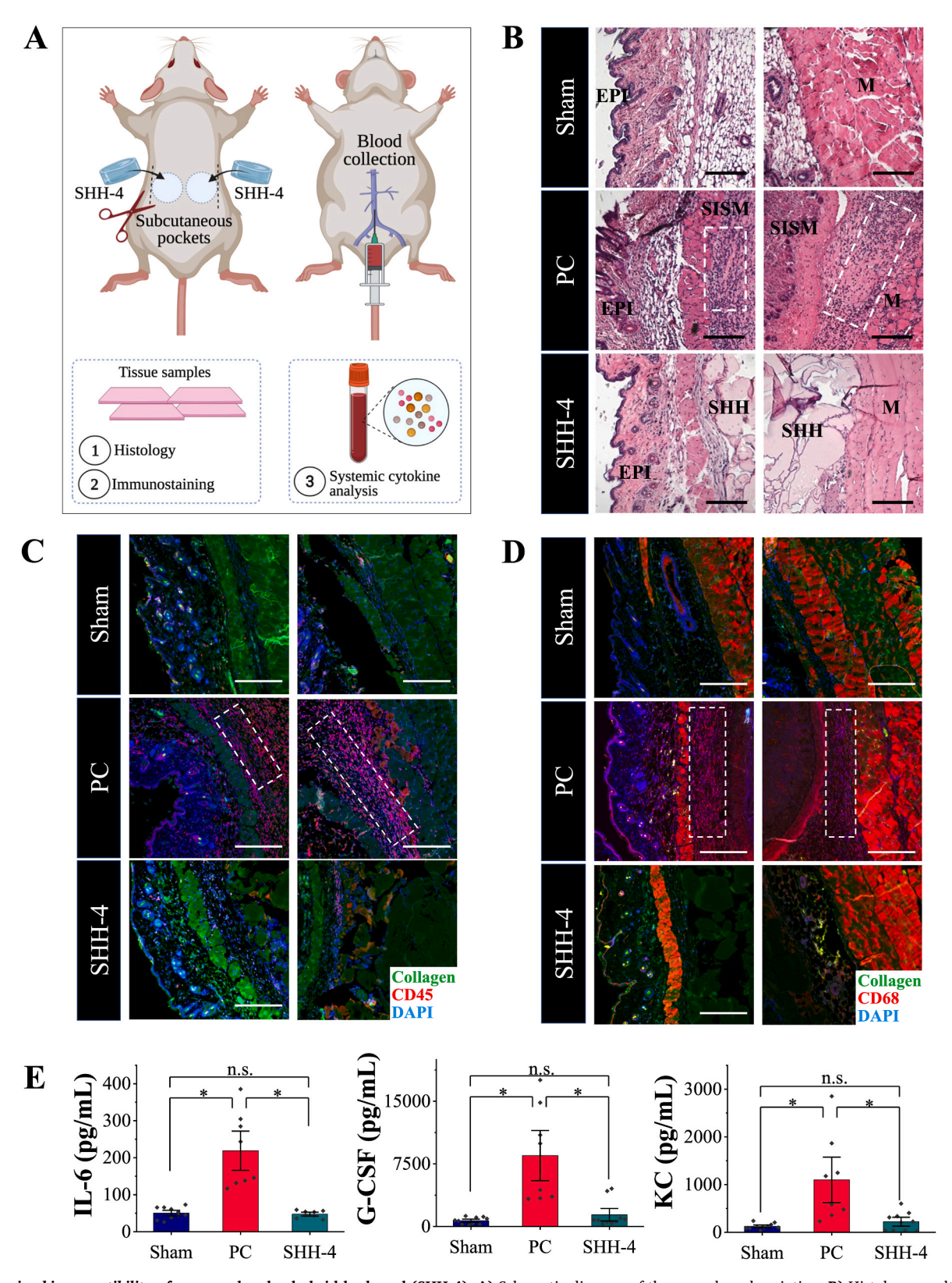


Fig. 7. In vivo biocompatibility of supramolecular hybrid hydrogel (SHH-4). A) Schematic diagram of the procedure description, B) Histology results for mice with and without SHH-4 treatment. EPI: Epidermis, M: Muscle, SISM: Small intestinal submucosa. Scale bar: 200  $\mu$ m. Immunofluorescence staining of mice tissue samples with C) CD45 and D) CD68. Scale bar: 300  $\mu$ m. E) in vivocirculating cytokine (bloodplasma) analysis for mice with and without SHH-4 treatment. Data are expressed as mean  $\pm$  SD. Sham control: A pocket was made, but no gel was implanted. Positive control: Small intestinal submucosa subcutaneously implanted to trigger immune response in mice. n=5 for negative control, n=5 for SHH-4, and n=4 for positive controls were used in the experiment. (IL-6: Interleukin 6, G-CSF: granulocyte colony-stimulating factor, and KC: keratinocyte chemoattractant. We use \*:  $p \le 0.05$ , n.s.: non-significant by Tukey-test for significance comparisons in E Fig. 7A was created with BioRender.com.

to provide easy burn care, eliminate mechanical and surgical debridement, promote wound healing, and enhance the healing process to treat second-degree burns. As a result, SHHs will reduce 1) pain and psychological burden of patients, 2) use and side effects of heavily used analgesics and opioids, 3) hospital stay and costs, and 4) time demand on highly qualified hospital personnel (i.e, doctors and nurse practitioners) by reducing the dressing change time significantly. To this end, we will follow up this study with investigations on the in vivo efficacy of SHHs in burn wound healing progress in large animal models with further SHH optimizations - via perturbations to the composition of existing formulations - and clinical trials to show the translatability of novel SHHs to the clinic. Further, we plan to conduct computational modeling studies, through collaborations, to further aid the optimization of the SHHs and gain further detailed insights into the interactions between the different components. We expect our invention to remove the challenges and shortcomings associated with current burn dressings and bear reduced pain, easy to apply, and removable burn dressings.

Beyond the targeted use of the SHHs as burn wound dressings in this study, SHHs may find many further uses in the broader areas of biomedical engineering, such as tissue and micro-tissue engineering, regenerative medicine, and biopreservation. SHHs could be further decorated with functional surface groups as needed for such purposes. The quick dissolubility of the SHHs would be especially desirable where sacrificial materials are useful for fabrication and/or as temporary closure elements. The tunable properties of SHHs can lend itself to cell and 3D tissue culture, where the specimens can first be fixed in space for imaging and observation in the SHHs but then released for detailed molecular analysis through the dissolution process under a minute, whereas alternatives take much longer. Such engineered tissue constructs may then also be useful both in the biopreservation of tissues and subsequent transplant applications in which our group and center are highly involved.

# Ethics approval and consent to participate

All protocols were in accord with the guidelines set by the Committee on Laboratory Resources, National Institutes of Health, and reviewed and approved by the Institutional Animal Care and Use Committee (IACUC) of Massachusetts General Hospital (Protocol number: 2015N000187).

#### CRediT authorship contribution statement

A. Aslihan Gokaltun: Conceptualization, Investigation, Methodology, Validation, Visualization, Formal analysis, Writing – original draft. Letao Fan: Investigation, Visualization, Validation, Writing – review & editing. Luca Mazzaferro: Investigation, Writing – review & editing. Delaney Byrne: Investigation. Martin L. Yarmush: Funding acquisition, Writing – review & editing, Resources. Tianhong Dai: Methodology, Resources. Ayse Asatekin: Conceptualization, Resources, Supervision, Funding acquisition, Writing – review & editing, Project administration. O. Berk Usta: Conceptualization, Resources, Supervision, Funding acquisition, Writing – review & editing, Project administration.

# **Declaration of competing interest**

The authors declare no competing financial or nonfinancial interests.

# Acknowledgements

This research was supported partially by grants from the National Institutes of Health (NIH 5R21GM136002, NIH 1R21GM141683, and NIH 5R01HL145031), National Science Foundation (NSF Grant CHE-1904465 and EEC-1941543), a Massachusetts General Hospital (MGH) Executive Committee on Research (ECOR) Interim Support Fund, and a

Shriners Hospital Research Grant (SHC 85125, and 85128). We also acknowledge the support and use of facilities at the Morphology and Imaging Shared Facility, and Regenerative Medicine Shared Facility provided at the Shriners Hospital for Children – Boston. The authors thank Dr. Basak Uygun for fruitful discussions on this work, Dr. David Wilbur for assistance with NMR data collection and analysis, Dr. Nicole Brousaides for the preparation of histology samples, Dr. Leon G. Leanse for his help in animal procurement and initial training in the animal protocol.

# Appendix A. Supplementary data

Supplementary data to this article can be found online at https://doi.org/10.1016/j.bioactmat.2022.09.003.

#### References

- S.N. Forjuoh, Burns in low- and middle-income countries: a review of available literature on descriptive epidemiology, risk factors, treatment, and prevention, Burns 32 (2006) 529–537, https://doi.org/10.1016/j.burns.2006.04.002.
- [2] M.D. Peck, G.E. Kruger, A.E. van der Merwe, W. Godakumbura, R.B. Ahuja, Burns and fires from non-electric domestic appliances in low and middle income countries Part I. The scope of the problem, Burns 34 (2008) 303–311, https://doi. org/10.1016/j.burns.2007.08.014.
- [3] M.D. Peck, Epidemiology of burns throughout the world. Part I: distribution and risk factors, Burns 37 (2011) 1087–1100, https://doi.org/10.1016/j. burns.2011.06.005.
- [4] A.M. Lachiewicz, C.G. Hauck, D.J. Weber, B.A. Cairns, D. van Duin, Bacterial infections after burn injuries: impact of multidrug resistance, Clin. Infect. Dis. 65 (2017) 2130–2136, https://doi.org/10.1093/cid/cix682.
- [5] K.W. McDermott, A.J. Weiss, A. Elixhauser, in Healthcare Cost and Utilization Project (HCUP) Statistical Briefs, 2006.
- [6] F.K. Field, M.D. Kerstein, Overview of wound healing in a moist environment, Am. J. Surg. 167 (1994) 2S–6S, https://doi.org/10.1016/0002-9610(94)90002-7.
- [7] D.L. James, M. Jowza, Principles of burn pain management, Clin. Plast. Surg. 44 (2017) 737–747, https://doi.org/10.1016/j.cps.2017.05.005.
- [8] C. Griggs, J. Goverman, E.A. Bittner, B. Levi, Sedation and pain management in burn patients, Clin. Plast. Surg. 44 (2017) 535–540, https://doi.org/10.1016/j. cps.2017.02.026.
- [9] J. Latarjet, M. Choinere, Pain in burn patients, Burns 21 (1995) 344–348, https://doi.org/10.1016/0305-4179(95)00003-8.
- [10] R.J. Alencar de Castro, P.C. Leal, R.K. Sakata, Pain management in burn patients, Braz. J. Anesthesiol. 63 (2013) 149–153, https://doi.org/10.1016/S0034-7094 (13)70206-X.
- [11] M.D. Konieczynska, et al., On-demand dissolution of a dendritic hydrogel-based dressing for second-degree burn wounds through thiol-thioester exchange reaction, Angew Chem. Int. Ed. Engl. 55 (2016) 9984–9987, https://doi.org/10.1002/ pxis.2016.04827.
- [12] W. Lu, et al., On-demand dissoluble diselenide-containing hydrogel, Biomacromolecules 21 (2020) 3308–3317, https://doi.org/10.1021/acs.
- [13] C. Ghobril, K. Charoen, E.K. Rodriguez, A. Nazarian, M.W. Grinstaff, A dendritic thioester hydrogel based on thiol-thioester exchange as a dissolvable sealant system for wound closure, Angew Chem. Int. Ed. Engl. 52 (2013) 14070–14074, https://doi.org/10.1002/anie.201308007.
- [14] M.D. Konieczynska, et al., A hydrogel sealant for the treatment of severe hepatic and aortic trauma with a dissolution feature for post-emergent care, Mater. Horiz. 4 (2017) 222–227, https://doi.org/10.1039/C6MH00378H.
- [15] S.S. Anumolu, et al., Doxycycline hydrogels with reversible disulfide crosslinks for dermal wound healing of mustard injuries, Biomaterials 32 (2011) 1204–1217, https://doi.org/10.1016/j.biomaterials.2010.08.117.
- [16] X. Xu, W. Lu, J. Zhu, X. Pan, X. Zhu, An on-demand dissoluble chitosan hydrogel containing dynamic diselenide bond, Gels 7 (2021), https://doi.org/10.3390/ gels7010021.
- [17] W. Huang, et al., On-demand dissolvable self-healing hydrogel based on carboxymethyl chitosan and cellulose nanocrystal for deep partial thickness burn wound healing, ACS Appl. Mater. Interfaces 10 (2018) 41076–41088, https://doi. org/10.1021/acsami.8b14526.
- [18] Katherine A. Cook, et al., In situ gelling and dissolvable hydrogels for use as ondemand wound dressings for burns, Biomater. Sci. 9 (2021) 6842–6850, https:// doi.org/10.1039/d1bm00711d.
- [19] W. Xu, Q. Song, J.F. Xu, M.J. Serpe, X. Zhang, Supramolecular hydrogels fabricated from supramonomers: a novel wound dressing material, ACS Appl. Mater. Interfaces 9 (2017) 11368–11372, https://doi.org/10.1021/acsami.7b02850.
- [20] M.D. Konieczynska, M.W. Grinstaff, On-demand dissolution of chemically crosslinked hydrogels, Acc. Chem. Res. 50 (2017) 151–160, https://doi.org/10.1021/ acs.accounts.6b00547.
- [21] J.C. Anderson, A.J. Blake, J.P. Graham, C. Wilson, Investigation of the asymmetric ionic Diels-Alder reaction for the synthesis of cis-decalins, Org. Biomol. Chem. 1 (2003) 2877–2885, https://doi.org/10.1039/b305116a.

- [22] A.D. Baldwin, K.L. Kiick, Reversible maleimide-thiol adducts yield glutathionesensitive poly(ethylene glycol)-heparin hydrogels, Polym. Chem. 4 (2013) 133–143, https://doi.org/10.1039/C2PY20576A.
- [23] P.M. Kharkar, K.L. Kiick, A.M. Kloxin, Design of thiol- and light-sensitive degradable hydrogels using michael-type Addition reactions, Polym. Chem. 6 (2015) 5565–5574, https://doi.org/10.1039/C5PY00750J.
- [24] H. Lu, et al., Recent advances of on-demand dissolution of hydrogel dressings, Burns Trauma 6 (2018) 35, https://doi.org/10.1186/s41038-018-0138-8.
- [25] X. Du, J. Zhou, J. Shi, B. Xu, Supramolecular hydrogelators and hydrogels: from soft matter to molecular biomaterials, Chem. Rev. 115 (2015) 13165–13307, https://doi.org/10.1021/acs.chemrev.5b00299.
- [26] X. Ma, Y. Zhao, Biomedical applications of supramolecular systems based on host-guest interactions, Chem. Rev. 115 (2015) 7794–7839, https://doi.org/10.1021/cr500392w.
- [27] S.M. Mantooth, B.G. Munoz-Robles, M.J. Webber, Dynamic hydrogels from host-guest supramolecular interactions, Macromol. Biosci. 19 (2019), e1800281, https://doi.org/10.1002/mabi.201800281.
- [28] K.I. Assaf, W.M. Nau, Cucurbiturils: from synthesis to high-affinity binding and catalysis, Chem. Soc. Rev. 44 (2015) 394–418, https://doi.org/10.1039/ c4cs00273c.
- [29] M.V. Rekharsky, et al., A synthetic host-guest system achieves avidin-biotin affinity by overcoming enthalpy-entropy compensation, Proc. Natl. Acad. Sci. U. S. A. 104 (2007) 20737–20742, https://doi.org/10.1073/pnas.0706407105.
- [30] E.A. Appel, et al., Ultrahigh-water-content supramolecular hydrogels exhibiting multistimuli responsiveness, J. Am. Chem. Soc. 134 (2012) 11767–11773, https://doi.org/10.1021/ja3044568.
- [31] X. Yan, F. Wang, B. Zheng, F. Huang, Stimuli-responsive supramolecular polymeric materials, Chem. Soc. Rev. 41 (2012) 6042–6065, https://doi.org/10.1039/ c20c35001b
- [32] L. Yang, X. Tan, Z. Wang, X. Zhang, Supramolecular polymers: historical development, preparation, characterization, and functions, Chem. Rev. 115 (2015) 7196–7239, https://doi.org/10.1021/cr500633b.
- [33] Q. Wang, et al., High-water-content mouldable hydrogels by mixing clay and a dendritic molecular binder, Nature 463 (2010) 339–343, https://doi.org/10.1038/ nature08693.
- [34] K. Haraguchi, T. Takehisa, Nanocomposite hydrogels: a unique organic-inorganic network structure with extraordinary mechanical, optical, and swelling/deswelling properties, Adv. Mater. 14 (2002) 1120–1124.
- [35] Z. Li, Z. Hou, H. Fan, H. Li, Organic-inorganic hierarchical self-assembly into robust luminescent supramolecular hydrogel, Adv. Funct. Mater. 27 (2017), 1604379.
- [36] D. Yang, et al., Color-tunable luminescent hydrogels with tough mechanical strength and self-healing ability, J. Mater. Chem. C 6 (2018) 1153–1159.
- [37] S. Tamesue, et al., Linear versus dendritic molecular binders for hydrogel network formation with clay nanosheets: studies with ABA triblock copolyethers carrying guanidinium ion pendants, J. Am. Chem. Soc. 135 (2013) 15650–15655, https:// doi.org/10.1021/ja408547g.
- [38] C. García-Astrain, et al., Green chemistry for the synthesis of methacrylate-based hydrogels crosslinked through Diels-Alder reaction, Eur. Polym. J. 49 (2013) 3998–4007, https://doi.org/10.1016/j.eurpolymj.2013.09.004.
- [39] C. Yang, et al., A green fabrication approach of gelatin/CM-chitosan hybrid hydrogel for wound healing, Carbohydr. Polym. 82 (2010) 1297–1305, https:// doi.org/10.1016/j.carbpol.2010.07.013.
- [40] Z. Wang, et al., Green gas-mediated cross-linking generates biomolecular hydrogels with enhanced strength and excellent hemostasis for wound healing, ACS Appl. Mater. Interfaces 12 (2020) 13622–13633, https://doi.org/10.1021/ cccqqi/0.01235
- [41] W. Mubarok, Y. Qu, S. Sakai, Influence of hydrogen peroxide-mediated cross-linking and degradation on cell-adhesive gelatin hydrogels, ACS Appl. Bio Mater. 4 (2021) 4184–4190, https://doi.org/10.1021/acsabm.0c01675.
- [42] J. Muhamed, D. Revi, A. Rajan, S. Geetha, T.V. Anilkumar, Biocompatibility and immunophenotypic characterization of a porcine cholecyst-derived scaffold implanted in rats, Toxicol. Pathol. 43 (2015) 536–545, https://doi.org/10.1177/ 0192623314550722
- [43] Z. Li, Y.M. Zhang, H. Wang, H. Li, Y. Liu, Mechanical behaviors of highly swollen supramolecular hydrogels mediated by pseudorotaxanes, Macromolecules 50 (2017) 1141–1146, https://doi.org/10.1021/acs.macromol.6b02459.
- [44] J.H. Lee, C. Kim, J.H. Jung, Control of the rheological properties of clay nanosheet hydrogels with a guanidinium-attached calix[4]arene binder, Chem. Commun. 51 (2015) 15184–15187, https://doi.org/10.1039/c5cc06024a.
- [45] D. Das, K.I. Assaf, W.M. Nau, Applications of cucurbiturils in medicinal chemistry and chemical biology, Front. Chem. 7 (2019) 619, https://doi.org/10.3389/ fchem.2019.00619.
- [46] S.J. Barrow, S. Kasera, M.J. Rowland, J. del Barrio, O.A. Scherman, Cucurbituril-based molecular recognition, Chem. Rev. 115 (2015) 12320–12406, https://doi.org/10.1021/acs.chemrev.5b00341.
- [47] A.J. Bullock, P. Pickavance, D.B. Haddow, S. Rimmer, S. MacNeil, Development of a calcium-chelating hydrogel for treatment of superficial burns and scalds, Regen. Med. 5 (2010) 55–64, https://doi.org/10.2217/rme.09.67.
- [48] M. Pawlaczyk, M. Lelonkiewicz, M. Wieczorowski, Age-dependent biomechanical properties of the skin, Adv. Dermatol. Allergol. Postepy Dermatol. i Alergol. 30 (2013) 302–306.

- [49] M.L. Crichton, X. Chen, H. Huang, M.A. Kendall, Elastic modulus and viscoelastic properties of full thickness skin characterised at micro scales, Biomaterials 34 (2013) 2087–2097.
- [50] A.T.K. Basti, et al., Employing cellulose nanofiber-based hydrogels for burn dressing, Polymers 14 (2022) 1207.
- [51] J.H. Lee, C. Kim, J.H. Jung, Control of the rheological properties of clay nanosheet hydrogels with a guanidinium-attached calix [4] arene binder, Chem. Commun. 51 (2015) 15184–15187.
- [52] J. Lagona, P. Mukhopadhyay, S. Chakrabarti, L. Isaacs, The cucurbit[n]uril family, Angew Chem. Int. Ed. Engl. 44 (2005) 4844–4870, https://doi.org/10.1002/ anie.200460675.
- [53] He, J. et al. Injectable self-healing adhesive pH-responsive hydrogels accelerate gastric hemostasis and wound healing. Nano-Micro Lett. 13, 80, doi:10.1007/ s40820-020-00585-0(2021).
- [54] J. Qu, et al., Antibacterial adhesive injectable hydrogels with rapid self-healing, extensibility and compressibility as wound dressing for joints skin wound healing, Biomaterials 183 (2018) 185–199, https://doi.org/10.1016/j. biomaterials.2018.08.044.
- [55] M. Chen, et al., Dynamic covalent constructed self-healing hydrogel for sequential delivery of antibacterial agent and growth factor in wound healing, Chem. Eng. J. 373 (2019) 413–424.
- [56] L. Zhao, et al., pH and glucose dual-responsive injectable hydrogels with insulin and fibroblasts as bioactive dressings for diabetic wound healing, ACS Appl. Mater. Interfaces 9 (2017) 37563–37574.
- [57] Z. Li, et al., Hydrogel cross-linked with dynamic covalent bonding and micellization for promoting burn wound healing, ACS Appl. Mater. Interfaces 10 (2018) 25194–25202.
- [58] D.L. Taylor, M. In Het Panhuis, Self-healing hydrogels, Adv. Mater. 28 (2016) 9060–9093, https://doi.org/10.1002/adma.201601613.
- [59] B. Zhang, J. He, M. Shi, Y. Liang, B. Guo, Injectable self-healing supramolecular hydrogels with conductivity and photo-thermal antibacterial activity to enhance complete skin regeneration, Chem. Eng. J. 400 (2020), 125994.
- [60] M.P. Ribeiro, et al., Development of a new chitosan hydrogel for wound dressing, Wound Repair Regen. 17 (2009) 817–824, https://doi.org/10.1111/j.1524-475X.2009.00538.x.
- [61] S. Ono, et al., Increased wound pH as an indicator of local wound infection in second degree burns, Burns 41 (2015) 820–824, https://doi.org/10.1016/j. burns.2014.10.023.
- [62] A. Kelso, Cytokines: principles and prospects, Immunol. Cell Biol. 76 (1998) 300–317. https://doi.org/10.1046/j.1440-1711.1998.00757.x.
- [63] J.M. Anderson, A. Rodríguez, D.T. Chang, Foreign body reaction to biomaterials, Semin. Immunol. 20 (2008) 86–100, https://doi.org/10.1016/j. smim 2007 11 004
- [64] D.F. Williams, On the mechanisms of biocompatibility, Biomaterials 29 (2008) 2941–2953, https://doi.org/10.1016/j.biomaterials.2008.04.023.
- [65] B.D. Ratner, The biocompatibility manifesto: biocompatibility for the twenty-first century, J. Cardiovasc. Transl. Res. 4 (2011) 523–527, https://doi.org/10.1007/ s12265-011-9287-x.
- [66] D.A. Boardman, et al., Expression of a chimeric antigen receptor specific for donor HLA class I enhances the potency of human regulatory T cells in preventing human skin transplant rejection, Am. J. Transplant. 17 (2017) 931–943, https://doi.org/ 10.1111/ajt.14185.
- [67] K. Ratnasothy, et al., IL-2 therapy preferentially expands adoptively transferred donor-specific Tregs improving skin allograft survival, Am. J. Transplant. 19 (2019) 2092–2100, https://doi.org/10.1111/ajt.15306.
- [68] Q. Zhai, et al., An immune-competent rat split thickness skin graft model: useful tools to develop new therapies to improve skin graft survival, Am. J. Transl. Res. 10 (2018) 1600–1610.
- [69] F. Ordikhani, V. Pothula, R. Sanchez-Tarjuelo, S. Jordan, J. Ochando, Macrophages in organ transplantation, Front. Immunol. 11 (2020), 582939, https://doi.org/ 10.3389/fimmu.2020.582939.
- [70] R. Di Liddo, et al., Histone deacetylase inhibitors restore IL-10 expression in lipopolysaccharide-induced cell inflammation and reduce IL-1beta and IL-6 production in breast silicone implant in C57BL/6J wild-type murine model, Autoimmunity (2016) 1–11, https://doi.org/10.3109/08916934.2015.1134510.
- [71] T.H. Price, G.S. Chatta, D.C. Dale, Effect of recombinant granulocyte colonystimulating factor on neutrophil kinetics in normal young and elderly humans, Blood 88 (1996) 335–340.
- [72] E. Shochat, V. Rom-Kedar, L.A. Segel, G-CSF control of neutrophils dynamics in the blood, Bull. Math. Biol. 69 (2007) 2299–2338, https://doi.org/10.1007/s11538-2007.
- [73] C. Schumacher, I. Clark-Lewis, M. Baggiolini, B. Moser, High- and low-affinity binding of GRO alpha and neutrophil-activating peptide 2 to interleukin 8 receptors on human neutrophils, Proc. Natl. Acad. Sci. U. S. A. 89 (1992) 10542–10546, https://doi.org/10.1073/pnas.89.21.10542.
- [74] D.T. Luttikhuizen, et al., The correlation between difference in foreign body reaction between implant locations and cytokine and MMP expression, Biomaterials 27 (2006) 5763–5770, https://doi.org/10.1016/j. biomaterials.2006.07.004.